Heliyon 10 (2024) e33642

Contents lists available at ScienceDirect

Heliyon

journal homepage: www.cell.com/heliyon

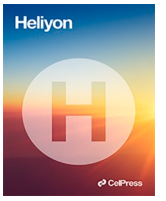

Research article

Exploring the potent hydrolytic activity of chitosan-cerium complex microspheres resin for organophosphorus pesticide degradation

Lina Yu [a], Yu Song [a], Jie Bi [a,**], Yuan Gao [a], Chen Jiang [a], Zhen Yang [a], Hongtao Qi [b], Honghua Yu [c], Weiqiang Yang [a], Qingxuan Gong [a], Chengren Shi [a], Mingqing Wang [a,*]

[a] Shandong Peanut Research Institute, Qingdao, 266100, PR China
[b] College of Life Sciences, Qingdao University, Qingdao, 266071, PR China
[c] Shandong Innovation and Entrepreneurship Community of Science and Technology Special Commissioner, Jinan, 250000, PR China

ARTICLE INFO

Keywords:
Chitosan-cerium complex microspheres resin
Characterization
Hydrolytic activity
Organophosphorus pesticides
Degradation

ABSTRACT

Chitosan is a biocompatible, non-toxic and renewable natural basic polysaccharide that can be cross-linked and reacted with Ce(IV) to form a physiologically active chitosan-Ce(IV) complex. To investigate this novel complex and its potential to hydrolyze phosphate ester bonds, chitosan-cerium complex microspheres resin (CS-CCMR) was prepared from chitosan and ceric ammonium nitrate by reversed-phase suspension cross-linking polymerization. CS-CCMR was characterized, its ability to hydrolyze disodium p-nitrobenzene phosphate (PNPP2Na) and organophosphorus pesticides was investigated, and the hydrolytic mechanism was explored. CS-CCMR was composed of dark yellow microspheres with smooth surfaces and dense pores. It was found that CS-CCMR contained 4.507 mg/g Ce(IV), indicating that coordination polymerization between Ce(IV) and chitosan was successful. The presence of Ce(IV) in CS-CCMR was confirmed by multiple analytical methods and it was found that coordination of Ce(IV) by chitosan was mediated by the nitrogen atom of the amino group and the oxygen atom of the hydroxyl group of chitosan. It was shown that CS-CCMR efficiently hydrolyzed the phosphate ester bonds of PNPP2Na and five organophosphorus pesticides. Hydrolysis of PNPP2Na is potentially accomplished by charge neutralization and nucleophilic substitution. The mechanism of parathion degradation by CS-CCMR involves modification of the nitro group to give aminoparathion, followed by cleavage of the P–O bond to generate diazinphos. Consequently, the novel chitosan-Ce(IV) complex exhibits great efficiency for hydrolysis of phosphate ester bonds and CS-CCMR is expected to be developed as an agent to reduce the possibility of contamination of fruit and vegetable drinks by organophosphorus pesticides.

* Corresponding author. Food Engineering Innovation Team, Shandong Peanut Research Institute, Qingdao, 266100, PR China.
** Corresponding author. Food Engineering Innovation Team, Shandong Peanut Research Institute, Qingdao, 266100, PR China.
E-mail addresses: bj.baby@163.com (J. Bi), Annabelle2010@163.com (M. Wang).

https://doi.org/10.1016/j.heliyon.2024.e33642
Received 18 March 2024; Received in revised form 25 June 2024; Accepted 25 June 2024
Available online 28 June 2024

1. Introduction

Chitosan is a polymer chain consisting of β-(1 → 4)-2-amino-2-deoxy-D-glucan and β-(1 → 4)-2-acetylamino-2-deoxy-D-glucan, which is obtained by deacetylation of chitin [1]. There are two hydrogen bonds in the chitosan chain: one between the C_3 hydroxyl and the C_5 oxygen atom and one between the C_6 hydroxyl and the amino group nitrogen atom [2]. Protonation of the $–NH_2$ functional group on C_2 of the D-glucosamine unit enables dissolution of chitosan in organic acids, such as acetic, formic and citric acids, and in hydrochloric acid [3]. Chitosan is converted into a polyelectrolyte in acidic medium and is the only natural alkaline polysaccharide [4]. Chitosan contains active amino, acetylamino and hydroxyl groups that are coordination and reaction sites [5]. These active functional groups can form stable chelating agents that coordinate with many heavy metal, transition metal or lanthanide ions.

One important application of chitosan is coordination with heavy metal ions, especially with Cu, Pb, Cd, Ni and Cr. In this way, chitosan can be used to remove toxic metal ions from contaminated aqueous wastes. Rahaman et al. used a modified cellulose and chitosan composite as adsorbent to treat wastewater polluted by Cr, Pb and Cd heavy metals [6]. The results showed that the composite adsorbent removed Cr, Pb and Cd by coordination, and the removal of Cd was greatest. In another study, a pore structure control agent (PSCA) was used to regulate the pore structure of chitosan hydrogels for rapid removal of Cr(VI), Cu(II) and Ni(II) from wastewater [7]. The total adsorption of the three heavy metal ions was greater than 750 mg/g. Kinetic studies showed that the chitosan gel exhibited physical adsorption of Cr(VI) and chemical adsorption of Cu(II) and Ni(II). In addition, chitosan coordinates with transition metal ions well. Shikha et al. obtained four chitosan-transition metal ion complexes by reaction of O-carboxymethyl chitosan (O-CMC) Schiff base with Zn(II), Ni(II), Fe(II) and Cu(II) [8]. The complexes were characterized by Fourier transform infrared (FTIR) spectroscopy, ^1H nuclear magnetic resonance (NMR) spectroscopy, X-ray powder diffraction (XRD), scanning electron microscopy (SEM), ultraviolet–visible spectroscopy and fluorescence spectroscopy, which showed that the structure of chitosan was changed. Moreover, the chitosan-transition metal complexes, especially the Fe and Zn complexes, exhibited good antibacterial activity. Shinde et al. found that among complexes of chitosan with transition metal ions such as Cu(II), Fe(III), La(III), Mo(VI) and Zr(IV), the complexes with Fe(III) and La(III) strongly adsorbed As(V) from water, and the chitosan-Fe(III) complex performed better than the chitosan-La(III) complex in adsorption of As(V) from seawater [9].

Cerium is a lanthanide and common electron donor atoms, such as oxygen, nitrogen and sulfur, can form coordination bonds with cerium ions. Chitosan is a β-(1 → 4)-linked biopolymer of 2-amino-2-deoxy-D-glucosamine repeat units, which can selectively form coordination compounds with cerium ions. Wujcicki et al. used modified chitosan-cerium hydrogels to adsorb phosphate(V) ions, and found that four times more was adsorbed compared with unmodified chitosan hydrogels [10]. In addition, the results showed improved physical and chemical adsorption capacities of cerium-modified chitosan. Alshahrani et al. prepared a novel chitosan-functionalized hydroxyapatite-cerium oxide heterostructure material [11]. This material can remove Congo red (CR) dyes from industrial wastewater and has potential antibacterial activity. It can be seen that complexes of chitosan and cerium ion have useful properties. The use of modified chitosan in coordination chemistry has numerous potential applications.

In general, chitosan is modified by glutaraldehyde before reaction with cerium ion to form a stable complex. Glutaraldehyde contains highly reactive aldehyde groups that can rapidly form Schiff bases with the amino groups of chitosan, generating a three-dimensional network structure [12–15]. This network structure not only increases the surface area for metal adsorption, but also increases the structural and chemical stability of the cross-linked product to resist the effects of acid on the inner and outer surfaces [16]. From the macroscopic point of view, cerium ions are adsorbed on the inside of the modified chitosan after complexation. From the microscopic point of view, physical or chemical interactions between the modified chitosan and cerium ion occur [17]. For example, the nitrogen atom of the C_2 amino group in chitosan can donate a lone pair of electrons to a cerium ion, resulting in adsorption of cerium ion on the chitosan particle after coordination [18,19]. In addition, the nitrogen atom of the Schiff base formed by cross-linking of chitosan can also provide an electron pair, which exerts an electrostatic attraction for cerium ion [20–22]. The relatively stable coordination of the nitrogen atom and cerium ion provides another mechanism for adsorption of cerium ion by the cross-linked chitosan particles.

It has been reported that cerium ion is able to hydrolyze both phosphate ester and peptide bonds. In one study, Du et al. prepared Ce-doped carbon dots (CeCD) by one-step hydrothermal carbonization, and used bis(4-nitrophenyl) phosphate (BNPP) as a model substrate to investigate its hydrolytic activity [23]. The results showed that CeCD acted as a phosphatase mimetic and exhibited good catalytic activity for BNPP hydrolysis. Further verifying its hydrolytic activity, CeCD gave 74.50 % degradation of the organophosphorus pesticide, chlorpyrifos. In another study, Takarada et al. found that Ce(IV) effectively hydrolyzed tripeptides and tetrapeptides [24]. Moreover, there was no oxidative cleavage during hydrolysis of the tripeptide, and hydrolysis only occurred at the amide bond near the N-terminus due to coordination of the terminal amino group and carboxylate by Ce(IV). Therefore, free cerium ion has good activity in the hydrolysis of phosphate ester and peptide bonds. However, the application of free cerium ions has great limitations. The biocompatibility and non-toxicity of chitosan and its coordination with metal ions suggest that chitosan-Ce coordination complexes can be prepared by combining chitosan with cerium ions. Thus, hydrolysis of phosphate ester and peptide bonds by cerium ion might be applied more widely.

However, at present, research on chitosan-cerium complexes is mainly focused on their antibacterial activity. For example, tea polyphenols mediated the activity of chitosan-coated cerium nanocomposite against *Escherichia coli*, *Staphylococcus aureus* and *Botrytis cinerea* [25]; cerium nanoparticle-chitosan composite film was active against *E. coli* and *S. aureus* [26]; chitosan-based cerium and titanium oxide loaded polycaprolactone was active against *E. coli* and *S. aureus* [27]; chitosan-cerium oxide porous scaffolds have an inhibitory effect on the bacteria growth and strains at the site of bone injury [28]. These chitosan-cerium complexes can be widely used in food, agricultural production, packaging materials, coating materials, wound dressings and biomedical fields.

With the development of agricultural production and trade, organophosphorus pesticides (OPPs) have been widely used in

agriculture in recent years [29]. At present, OPPs are extensively used in different crops such as fruits, vegetables, tea and cereal grains to reduce and control pests [30–33]. The application of OPPs can increase the yield of agricultural product and realize the sustainable development of agriculture. However, non-standard operation results in OPPs residue in fruits, vegetables, tea and other agricultural products [34–36]. In addition, with the water circulation, OPPs will residue in the water source [37,38]. If OPPs residue in some related products, such as fruit and vegetable juice, tea, it will bring potential harm to food safety and human health. Therefore, the degradation and removal of OPPs residues in fruit and vegetable juices and drinking water is a key problem. It will encourage researchers to develop new, simple and effective methods for degradation of OPPs. Chitosan is a biocompatibility polymer, and cerium has the potential to hydrolyze phosphate ester bonds and peptide bonds. It is suggested that chitosan and cerium can be prepared into a stable and reusable chitosan-cerium complex microsphere resins. Their application in the removal of OPPs in fruit and vegetable juices, and drinking water will make a significant contribution to agricultural products and food safety. In view of this, in this study, chitosan-cerium complex microspheres resin (CS-CCMR) was prepared by reversed-phase suspension cross-linking polymerization using chitosan as ligand, Ce(IV) from ceric ammonium nitrate as coordination ion and glutaraldehyde as cross-linking agent. The physicochemical properties of CS-CCMR were determined, and the hydrolytic activities of CS-CCMR toward disodium p-nitrobenzene phosphate (PNPP2Na) and organophosphorus pesticides were investigated. The purpose of this study was to provide a method for development of a chitosan-Ce(IV) complex for hydrolysis of phosphate ester bonds, and to provide a theoretical basis for its application in food and agricultural industries.

2. Experimental

2.1. Chemical reagents

Four kinds of chitosan with different viscosity average molecular weight and deacetylation degree (DDA), they are 5.1×10^5 and 80 %, 5.3×10^5 and 85 %, 5.1×10^5 and 90 %, 5.1×10^7 and 85 %, respectively, were provided by Lizhong Chitosan Company Limited, Qingdao, China. Ammonium ceric nitrate was analytical reagent produced by Shanghai Shanpu Chemical Co., Ltd., Shanghai, China. Acetic acid, liquid paraffin, ethyl acetate, Span-80, formaldehyde solution, 50 % glutaraldehyde solution, petroleum ether (boiling range 60–90 °C), acetone, anhydrous ethanol, were analytical reagents produced by Sinopharm Chemical Reagent Co., Ltd., Shanghai, China. Disodium p-nitrobenzene phosphate (PNPP2Na) was analytical reagent produced by Sigma-Aldrich Co., Ltd., Shanghai, China. Dichlorvos was 77.5 % emulsion formulation produced by Zhengzhou Leslier Agrochemical Co., Ltd., Zhengzhou, China. Omethoate was 40 % emulsion formulation produced by Wuhan Hannan Concentric Chemical Co., Ltd., Wuhan, China. Dimethoate was 50 % emulsion formulation produced by Qingdao Lier Agrochemical (Group) R & D Co., Ltd., Qingdao, China. Chlorpyrifos was 48 % emulsion formulation produced by Guangzhou Belka Biotechnology Co., Ltd., Guangzhou, China. Parathion was 50 % emulsion formulation produced by Beining Pesticide Factory, Jinzhou, China. All other reagents were of analytical reagents and used as received.

2.2. Preparation of CS-CCMR and CSMR

The preparation of CS-CCMR was carried out according to the method of Yu et al. [39]. CS-CCMR was prepared by reversed-phase suspension cross-linking polymerization. The technology consists of six steps: dispersion, emulsification, pre-crosslinking, cross--linking, washing and drying. First, ceric ammonium nitrate (1.5 % *w/v*) was dissolved in aqueous acetic acid (2 % *v/v*), and then chitosan (5 % *w/v*) was dissolved in this solution to form a chitosan-ceric ammonium nitrate-acetic acid solution. The mixed solution was poured into liquid paraffin (dispersant) at a ratio of 1:1 (*v/v*). The mixture was electrically agitated for 10 min at 300 r/min to uniformly disperse the solution in the liquid paraffin. Secondly, Span-80 (emulsifier, 0.6 % *v/v*) was added to the reaction solution dropwise with a rubber head dropper, followed by addition of ethyl acetate (porogen, 10 % *v/v*). The mixture was stirred at 500 r/min and a constant temperature of 50 °C for 20 min to form small droplets in the emulsion. Thirdly, formaldehyde solution (10 % *v/v*) was added to the reactant solution and stirred for 30 min at 500 r/min and a constant temperature of 60 °C. Thus, under acidic conditions, some of the amino groups on chitosan cross-linked with formaldehyde. Fourthly, 5 % (*v/v*) glutaraldehyde solution (50 %, *v/v*) was added to the reaction solution and stirred at 175 r/min and 70 °C. After adjusting the pH value of the emulsion using 2.0 mol/L aqueous NaOH solution, the emulsion was stirred for 3 h. Then, under neutral or weak alkaline conditions, the two aldehydes of glutaraldehyde and the chitosan amino or acetylamino groups cross-linked to form intramolecular or intermolecular Schiff bases. Fifth, CS-CCMR was obtained by filtering the mixture under vacuum. The CS-CCMR was heated in petroleum ether at 60 °C for 12 h and then the suspension was cooled and filtered. The CS-CCMR was washed successively with acetone, absolute ethanol and distilled water. Finally, the CS-CCMR was dried under vacuum at 50 °C.

The preparation of CSMR was carried out according to the method of Yu et al. [40]. For the preparation of CSMR, 5 % (*w/v*) chitosan was directly dissolved in 2 % (*v/v*) acetic acid solution instead of ceric ammonium nitrate-acetic acid solution. The other steps were the same as those for preparation of CS-CCMR.

2.3. Single factor experiment method

2.3.1. Effect of chitosan with different DDA on preparation CS-CCMR

Chitosan with different DDA were used as raw materials to prepare CS-CCMR under the following conditions: chitosan viscosity average molecular weight of about 5.0×10^5; DDA of 80 %, 85 % or 90 %; 1.5 % (*w/v*) ceric ammonium nitrate; reaction solution pH of

7.0.

2.3.2. Effect of chitosan with different viscosity-average molecular weights on preparation CS-CCMR

CS-CCMR was prepared from two variants of chitosan with viscosity-average molecular weights of 5.0×10^5 (M_wL) and 5.0×10^7 (M_wH). The other reaction conditions were as follows: 85 % DDA chitosan; 1.5 % (*w/v*) ceric ammonium nitrate; reaction solution pH of 7.0.

2.3.3. Effect of different amounts of ceric ammonium nitrate on preparation CS-CCMR

The experimental conditions for preparation of CS-CCMR using different amounts of ceric ammonium nitrate were as follows: chitosan viscosity-average molecular weight of 5.0×10^5; 85 % DDA chitosan; 0.5 %, 1.0 %, 1.5 % or 2.0 % (*w/v*) ceric ammonium nitrate; reaction solution pH of 7.0.

2.3.4. Effect of different pH values on preparation CS-CCMR

CS-CCMR was prepared at different pH values (6.5, 7.0, 7.5 or 8.0), using chitosan with viscosity-average molecular weight of 5.0×10^5 and 80 % DDA, and 1.5 % (*w/v*) ceric ammonium nitrate.

2.4. Determination of physical properties

Physical properties, including moisture content, cross-linking degree, pile-up density, skeleton density, pore degree, free aldehyde groups, and weak basic exchange capacities of CS-CCMR and CSMR were determined using the methods of Yu et al. [41].

2.4.1. Determination of moisture content

A 0.1 g sample was fully swelled in water and filtered. The surface of the sample was blotted with absorbent paper and weighed (G_1, g). The sample was then dried at 105 °C for 4 h in a constant temperature drying chamber and weighed again (G_2, g). The moisture content (H, %) was calculated according to formula (1):

$$H(\%) = \frac{G_1 - G_2}{G_1} \times 100 \tag{1}$$

2.4.2. Determination of cross-linking degree

Samples (0.25 g, W_1) were soaked in 2 % (*v/v*) acetic acid solution for 24 h and then dried at 105 °C for 4 h in a constant temperature dryer and weighed (W_2, g). The cross-linking degree (ξ, %) was calculated according to formula (2):

$$\xi(\%) = \frac{W_1 - W_2}{W_1} \times 100\% \tag{2}$$

2.4.3. Determination of pile-up density

Pile-up density refers to the weight of a sample per unit volume, including the volumes of the skeleton, pores and voids between spheres. The mass (W, g) of about 2 mL (V_P) sample was measured in a 10 mL tube. The pile-up density (ρ_p, g/mL) was calculated according to formula (3):

$$\rho_P(\mathrm{g/mL}) = \frac{W}{V_P} \tag{3}$$

2.4.4. Determination of skeleton density

n-Heptane (5 mL) was added to a 10 mL measuring tube, weighed (W_1, g), and then discarded. The sample (0.1 g, W) was added to the measuring tube, followed by n-heptane (2 mL). After standing for 2 h, n-heptane was added to 5 mL and then the tube was weighed (W_2, g). The skeleton volume (V_T, mL) was calculated according to formula (4):

$$V_T = \frac{W_1 - W_2 + W}{dt} \tag{4}$$

where dt is the density of n-heptane, 0.6830 g/cm^3. Then, skeleton density (ρ_T, g/cm^3) was calculated according to formula (5):

$$\rho_T(g/cm^3) = \frac{W}{V_T} \tag{5}$$

2.4.5. Determination of pore degree

Pore degree (P) was calculated according to the following formula (6), where ρ_T and H are skeleton density and moisture content, respectively:

$$P = \frac{\rho_T \times H}{\rho_T \times H + 1 - H} \tag{6}$$

2.4.6. Determination of free aldehyde group content

Sample (0.1 g) was fully swelled in water and excess water removed by filtration. The sample was then oscillated with hydroxylamine (10.0 mL) at room temperature for 1 h. Then two drops of 0.05 % bromophenol blue indicator were added and titrated to the end point with standard hydrochloric acid solution (0.02 mol/L). Free aldehyde group content (mmol/g) was calculated from the following formula (7), where N (mol/L) is the concentration of standard hydrochloric acid solution, V_0 (mL) is the volume of standard hydrochloric acid consumed by the blank, V_1 (mL) is the volume of standard hydrochloric acid consumed by the sample, and W (g) is the weight of the sample:

$$\text{Free aldehyde group content}\ (\text{mmol}/\text{g}) = \frac{N \times (V_0 - V_1)}{W} \tag{7}$$

2.4.7. Determination of weak basic exchange capacity

Sample (0.1 g) was fully swelled in water and excess water removed by vacuum filtration. The sample was then agitated in standard hydrochloric acid solution (20 mL, 0.05 mol/L) at room temperature for 1 h. Subsequently, 15.0 mL of supernatant was treated with two drops of 0.2 % phenolphthalein indicator and titrated to the end point with standard sodium hydroxide solution (0.05 mol/L). Weak basic exchange capacity (mmol/g) was calculated from the following formula (8), where N_1 (mol/L) and N_2 (mol/L) are the concentrations of the standard hydrochloric acid and sodium hydroxide solutions, respectively, V_1 (mL) and V_2 (mL) are the volumes of the standard hydrochloric acid and sodium hydroxide solutions, respectively, and W (g) is the weight of the sample.

$$\text{Exchange capacity of weak base}\ (\text{mmol}/\text{g}) = \frac{N_1 \times V_1 - N_2 \times V_2 \times \frac{20}{15}}{W} \tag{8}$$

2.5. Structure and thermal stability characterization

2.5.1. Sample appearance picture and particle size analysis

Morphology of sample was analyzed by scanning electron microscopy (SEM) (JSM-840, Japanese Electronics Co., Ltd., Tokyo, Japan) and super depth of field three-dimensional microscopy system (VHX-950F, KEYENCE, Osaka, Japan). Particle size distribution of sample was determined by laser diffraction particle size analyzer (LS200, Beckman Coulter, Inc., Fullerton, USA).

2.5.2. Analysis of rare earth elements, carbon, nitrogen and hydrogen in samples

Rare earth elements in the samples were determined by Inductively Coupled Plasma Optical Emission Spectrometer (ICP-OES) (iCAP7000, Thermo Fisher Scientific Inc., Waltham, USA). The determination of carbon, nitrogen and hydrogen was carried out by element analyzer (Vario EL III, Elementar Analysensysteme GmbH, Hanau, Germany).

2.5.3. Fourier transform infrared (FTIR) spectrometric analysis

The FTIR spectra of samples were determined by fourier transform infrared spectrometer (Nicolet NEXUS 470, Thermo Nicolet Corporation, Madison, USA), and their structural characteristics were analyzed. Samples were mixed with KBr at a ratio of 1:100. Under the protection of infrared lamp, agate mortar grinding into fine powder, and then manually press into the middle of the transparent sheet. The scanning wavelength range is 4000-400 cm^{-1}, and FTIR spectra are obtained at the speed of 2 cm^{-1}.

2.5.4. X-ray diffraction (XRD) analysis

The XRD intensity curves of samples were measured by X-ray diffractometer (Rigaku D/MAX 2500, Rigaku Corporation, Tokyo, Japan), and the changes of their crystal structures were analyzed. With Cu as the target, the scanning angle of 2θ is 5–50°, and the scanning speed of Kα-ray is 20min^{-1}.

2.5.5. Differential scanning calorimetry (DSC) analysis

DSC curves of samples were determined by differential scanning calorimeter (200 PC, NETZSCH-Gerätebau GmbH, Selb, Germany), and their thermal stability was analyzed. The sample is placed in a standard aluminum crucible, the cap is pressed with a capper, and a small hole is drilled in the cap to allow moisture to be extracted from the sample. An empty aluminum crucible was placed in the sample pool as a blank control. Sample is about 10 mg, heating temperature is from 20 °C to 400 °C, heating rate is 10 °C/min, cooling gas is 20 mL/min of nitrogen.

2.6. Hydrolytic activity studies

2.6.1. Study of PNPP2Na hydrolysis

Sample (0.1 g) was added to 3 mmol/L PNPP2Na solution (10 mL), oscillated at 30 °C for 2 h, and then the absorbance of the solution was measured at 405 nm. The 3 mmol/L PNPP2Na solution without sample was treated under the same conditions and the absorbance measured. The number of experiment replicates performed was in triplicate, and the data and errors were calculated by Microsoft Excel (Microsoft Office Professional Plus 2010).

2.6.2. Study of organophosphorus pesticide hydrolysis

Sample (0.1 g) was added to organophosphorus pesticide solution (10 mL), and the concentration of pesticide was determined by GC before and after oscillation at 30 °C for 24 h. The number of experiment replicates performed was in triplicate, and the data and errors were calculated by Microsoft Excel (Microsoft Office Professional Plus 2010). The degradation products were detected by GC-MS. The concentration of organophosphorus pesticide solution without sample was determined by GC before and after treatment under the same conditions.

2.7. Statistical analysis

All experiments were performed in triplicate and data were expressed as means and standard deviations. The SPSS Statistics 17.0 software (IBM Inc., Armonk, NY, USA) was used to analyze the variance of the results with the method of least significant difference (LSD).

3. Results and discussion

3.1. Single factor experimental results of CS-CCMR preparation

During preparation of CS-CCMR, the degree of deacetylation (DDA) and viscosity-average molecular weight of chitosan, the amount of ceric ammonium nitrate and the pH of the reaction solution have great effects on the physical properties and activity of CS-CCMR. Therefore, CS-CCMR was prepared while changing these four conditions, and the physical properties and hydrolytic activity of the products toward PNPP2Na were compared.

3.1.1. CS-CCMR prepared from different DDA chitosan

Table 1 shows that the moisture content and skeleton density increased as the DDA was increased. This is because high-DDA chitosan contains more free amino groups than low-DDA chitosan, and water bound to free amino groups is also greater [42]. However, there was no significant difference in pore degree or pile-up density among the three CS-CCMR samples. The cross-linking degree of CS-CCMR prepared using 80 % DDA chitosan was significantly higher than that of the other two samples ($p < 0.05$). The maximum skeleton density was obtained when CS-CCMR was prepared using 90 % DDA chitosan ($p < 0.05$). The hydrolytic activity of CS-CCMR prepared using 80 % or 85 % DDA chitosan was significantly higher than that prepared using 90 % DDA chitosan ($p < 0.05$).

3.1.2. CS-CCMR prepared from chitosan with different viscosity-average molecular weight

All of the parameters were higher for CS-CCMR prepared using M_wH than for CS-CCMR prepared using M_wL (Table 2). It can be concluded that M_wH contains more amino and acetylamino groups, and CS-CCMR prepared from M_wH also contains more active amino and acetylamino groups [43]. Apart from some amino and acetylamino groups that are cross-linked with formaldehyde and glutaraldehyde to form Schiff bases, other amino and acetylamino groups are available to adsorb water molecules or form complexes with Ce (IV). Although the hydrolytic activity of CS-CCMR prepared from M_wH was higher than that prepared from M_wL, M_wH-chitosan did not easily dissolve in the reaction solution, so the preparation of CS-CCMR was more difficult. Consequently, subsequent experiments were conducted using M_wL chitosan as the raw material.

3.1.3. CS-CCMR prepared using different amounts of ceric ammonium nitrate

From Table 3, the hydrolytic activity and skeleton density of CS-CCMR prepared using 2.0 % (*w/v*) ceric ammonium nitrate were significantly higher than those prepared using the other samples. The other four indexes were significantly lower than those prepared using the other samples ($p < 0.05$). When Ce(IV) is complexed with chitosan, it has hydrolytic activity toward PNPP2Na, breaking the phosphate ester bonds to form *p*-nitrophenol [44]. *p*-Nitrophenol has an absorption peak at 405 nm, so the hydrolytic activity can be determined by measuring absorption at that wavelength. When 2.0 % (*w/v*) ceric ammonium nitrate was added to the dissolved chitosan, the Ce(IV) content in the prepared CS-CCMR was higher, so its hydrolytic activity was also higher.

3.1.4. CS-CCMR prepared at different pH values

It can be seen from Table 4 that the hydrolytic activity of CS-CCMR prepared at pH 7.5 was significantly higher than those of the other samples ($p < 0.05$). The primary amino groups of chitosan are nucleophilic, and when they are deprotonated at pH > 7.0, the unshared electron pair readily interacts with Ce(IV) and water molecules [10,45]. At pH 8.0, moisture content, skeleton density and

Table 1
Physical properties and hydrolytic activities of CS-CCMR prepared from chitosan with different DDA.

DDA (%)	Moisture content (%)	Cross-linking degree (%)	Pile-up density (g/mL)	Skeleton density (g/cm^3)	Pore degree	Hydrolytic activity absorbance (A)
80	46.980^{c}±0.581	15.467^{a}±0.462	0.757^{a}±0.054	1.733 ^{b} ± 0.447	0.599^{a}±0.069	0.413^{a}±0.032
85	52.927 ^{b} ± 0.851	10.933^{c}±1.007	0.640^{a}±0.064	1.600 ^{b} ± 0.057	0.643^{a}±0.008	0.420^{a}±0.102
90	56.478^{a}±3.524	14.267 ^{b} ± 0.833	0.815^{a}±0.030	3.699^{a}±0.290	0.827^{a}±0.011	0.328 ^{b} ± 0.018

Note: Different superscript letters in each of indicators mean significant differences at 0.05 level ($p < 0.05$, $n = 3$).

Table 2
Physical properties and hydrolytic activities of CS-CCMR prepared from chitosan with different viscosity-average molecular weights.

Viscosity-average molecular weight	Moisture content (%)	Cross-linking degree (%)	Pile-up density (g/mL)	Skeleton density (g/cm^3)	Pore degree	Hydrolytic activity absorbance (A)
M_wL	52.927 ± 0.851	10.933 ± 1.007	0.640 ± 0.064	1.600 ± 0.057	0.643 ± 0.008	0.420 ± 0.102
M_wH	58.598 ± 3.590	11.867 ± 0.611	0.802 ± 0.005	2.784 ± 0.910	0.789 ± 0.051	0.659 ± 0.040

Table 3
Physical properties and hydrolytic activities of CS-CCMR prepared using different amounts of ceric ammonium nitrate.

Amount of ceric ammonium nitrate (%)	Moisture content (%)	Cross-linking degree (%)	Pile-up density (g/mL)	Skeleton density (g/cm^3)	Pore degree	Hydrolytic activity absorbance (A)
0.5	51.067^{a}±1.450	18.533^{a}±0.231	0.693 ^{b} ± 0.049	2.283^{a}±0.270	0.703^{a}±0.026	0.362 ^{d} ± 0.068
1.0	48.004 ^{b} ± 1.218	17.467 ^{b} ± 0.611	0.800 ^{ab} ± 0.119	1.313^{c}±0.081	0.548^{c}±0.016	0.490 ^{b} ± 0.077
1.5	46.980^{c}±0.581	15.467^{c}±0.462	0.757 ^{ab} ± 0.054	1.733 ^{b} ± 0.447	0.599 ^{b} ± 0.069	0.413^{c}±0.032
2.0	45.919 ^{d} ± 0.665	13.467 ^{d} ± 0.462	0.834^{a}±0.048	1.415^{c}±0.280	0.542^{c}±0.052	0.653^{a}±0.132

Note: Different superscript letters in each of indicators mean significant differences at 0.05 level ($p < 0.05$, $n = 3$).

Table 4
Physical properties and hydrolytic activities of CS-CCMR prepared at different pH values.

pH	Moisture content (%)	Cross-linking degree (%)	Pile-up density (g/mL)	Skeleton density (g/cm^3)	Pore degree	Hydrolytic activity absorbance (A)
6.5	52.262 ^{b} ± 0.552	10.533 ^{b} ± 0.231	0.745^{a}±0.065	1.369^{c}±0.260	0.597^{c}±0.044	0.337 ^{d} ± 0.027
7.0	46.980^{c}±0.581	15.467^{a}±0.462	0.757^{a}±0.054	1.733 ^{b} ± 0.447	0.599^{c}±0.069	0.413^{c}±0.032
7.5	51.971 ^{b} ± 0.995	10.400 ^{b} ± 0.693	0.725^{a}±0.035	1.784 ^{b} ± 0.375	0.654 ^{b} ± 0.052	0.690^{a}±0.013
8.0	55.960^{a}±0.584	9.333^{c}±0.462	0.624 ^{b} ± 0.053	2.159^{a}±0.572	0.726^{a}±0.054	0.473 ^{b} ± 0.004

Note: Different superscript letters in each of indicators mean significant differences at 0.05 level ($p < 0.05$, $n = 3$).

the pore degree of CS-CCMR were significantly higher than those of the other samples ($p < 0.05$). However, the yield and hydrolytic activity were lower than those of CS-CCMR prepared at pH 7.5.

3.2. Orthogonal experimental results of CS-CCMR preparation

$L_9(3^3)$ orthogonal experiments were carried out to optimize the preparation of CS-CCMR. On the basis of single factor experiments, chitosan with viscosity average molecular weight of about 5×10^5 was used as raw material; pH value, amount of ceric ammonium nitrate and DDA were used as the factors, and hydrolytic activity was used as the index. The $L_9(3^3)$ orthogonal experimental design and results of the range analysis are shown in Table 5.

The range analysis showed that the optimum process conditions were: pH 7.5, 2.0 % (*w/v*) ceric ammonium nitrate, and 85 % DDA; namely, the A3B3C2 experimental combination (Table 5). However, group 7 (A3B1C2) exhibited the highest hydrolytic activity. The order of importance of each factor was A, C, B. The analysis of variance results are shown in Table 6.

Table 5
$L_9(3^3)$ orthogonal experimental design and results of the range analysis.

	pH value	Amount of ceric cmmonium nitrate (%, w/v)	DDA (%)	Error	Hydrolytic activity absorbance (A)
	A	B	C	D	
1	1(6.5)	1(1.0)	1(80)	1	0.141 ± 0.013
2	1(6.5)	2(1.5)	2(85)	2	0.101 ± 0.012
3	1(6.5)	3(2.0)	3(90)	3	0.192 ± 0.017
4	2(7.0)	1(1.0)	3(90)	2	0.236 ± 0.043
5	2(7.0)	2(1.5)	1(80)	3	0.135 ± 0.026
6	2(7.0)	3(2.0)	2(85)	1	0.403 ± 0.034
7	3(7.5)	1(1.0)	2(85)	3	0.413 ± 0.036
8	3(7.5)	2(1.5)	3(90)	1	0.360 ± 0.011
9	3(7.5)	3(2.0)	1(80)	2	0.196 ± 0.032
K_{1j}	0.434	0.790	0.472	0.904	T = 2.177
K_{2j}	0.774	0.596	0.917	0.533	
K_{3j}	0.969	0.791	0.788	0.740	
R	0.535	0.195	0.445	0.371	

Table 6
Analysis of variance results.

Source	Sum of Deviations Squares	Freedom Degree	Variance	F	Fa	Significance
A	0.048	2	0.024	2.00	$F_{0.05}(2,4) = 6.94$	a
B△	0.008	2	0.004	0.33	$F_{0.01}(2,4) = 18.0$	/
C	0.035	2	0.018	1.50		b
Error	0.023	2	0.012	/	/	/
Error△	0.031	4	/	/	/	/
Sum	0.114	8	/	/	/	/

Note.
[a] Mean highly significant difference at 0.01 level ($p < 0.01$).
[b] Means significant difference at 0.05 level ($p < 0.05$).

According to the analysis variance (Table 6), the effect of factor A on hydrolytic activity was highly significant ($p < 0.01$), that of factor C was significant ($p < 0.05$), and that of factor B was not significant ($p > 0.05$). The F value of each factor showed that $F_A > F_C > F_B$, indicating that the order of effect of each factor on hydrolytic activity was A > C > B. For factor B, the change of level had little effect on the experimental results. Therefore, from an economic point of view, B1 should be chosen. So, the optimal level combination was A3B1C2, that is, pH 7.5, 1.0 % (*w/v*) ceric ammonium nitrate, and 85 % DDA chitosan. This optimal combination coincides with the design of the seventh group, which is the best of the nine groups in the orthogonal table. Therefore, this combination was selected as the optimal conditions.

The physical properties of nine groups of samples from the orthogonal experiments are shown in Table 7. The pore degree of each sample was 0.550–0.750, cross-linking degree was 6.000%–10.500 %, and moisture content was 50.336%–60.300 %. The results showed that CS-CCMR was porous, cross-linked and had good water swelling properties. The cross-linking property of CS-CCMR gives the resin a certain skeleton structure, conferring a particular three-dimensional conformation and rigid characteristics. Farasati Far et al. obtained cross-linked porous hydrogels by the reaction of chitosan with gelatin, formaldehyde and metal salt (Ag, Cu, and Zn) [46]. In this paper, CS-CCMR prepared by the reaction of chitosan with glutaraldehyde, formaldehyde and cerium is as cross-linked porous as the hydrogels mentioned above. The porous nature of the resin enables it to bind water. At the same time, because of the cross-linking, the resin does not absorb excessive amounts of water that would destroy its three-dimensional structure. This property is similar to the swelling property of chitosan/polyacrylic acid/octadecene (CS/PAA/ODE) double-crosslinked network hydrogel functionalized porous silica microspheres prepared by Luo et al. [47]. The hydrogel porous microspheres can't be too swelling, so it can be used as a liquid chromatography stationary phase. From their common swelling properties, it is suggested that CS-CCMR has the potential to filter liquid media.

3.3. Characterization of CS-CCMR

3.3.1. Basic physical properties of CS-CCMR

SEM and three-dimensional super depth of field microscopy images of CS-CCMR are shown in Fig. 1. (a) and (b). CS-CCMR is composed of dark yellow, dense and porous microspheres with smooth surfaces. The particle size distribution was measured using a laser diffraction particle size analyzer (Fig. 2.). The results showed an average particle size of 363.013 μm. All particles were less than 724.436 μm, while the 90 %, 50 % and 10 % CS-CCMR particle sizes were less than 554.182, 354.917 and 257.866 μm, respectively. The average particle size of chitosan microspheres resin (CSMR) prepared by reverse suspension cross-linking polymerization was 416.737 μm, so the average particle size of CS-CCMR was smaller than that of CSMR. In the preparation of CS-CCMR, the amino and hydroxyl groups of chitosan not only react with the aldehyde group of glutaraldehyde, but also interact with Ce(IV). Therefore, the structure of CS-CCMR is more compact and the particle size is smaller. The effect of particle size of chitosan/silver nanoparticle composite microspheres (CAgMs) on its activity was investigated by Liang et al. [48]. They found that silver concentration, glass transition temperature and hydrogen bond network of small size CAgMs were increased, indicating a high antimicrobial activity. In view of this, particle size of CS-CCMR is smaller than that of CSMR, suggesting that the potential activity of CS-CCMR should be further

Table 7
Physical properties of CS-CCMR.

	Moisture content (%)	Cross-linking degree (%)	Pile-up density (g/mL)	Skeleton density (g/cm^3)	Pore degree
1	53.097 ^{g} ± 0.297	6.667 ^{h} ± 0.611	0.899 ^{h} ± 0.131	1.796^{a}±0.720	0.656 ^{ab} ± 0.080
2	50.791 ^{h} ± 0.455	9.200 ^{b} ± 0.693	0.804 ^{de} ± 0.058	1.765^{a}±0.665	0.654 ^{ab} ± 0.077
3	57.153^{e}±0.836	7.467 ^{g} ± 0.231	0.879 ^{ab} ± 0.072	1.551 ^{bc}±0.280	0.671 ^{ab} ± 0.040
4	58.850 ^{b} ± 0.339	8.000 ^{d} ± 0.400	0.789^{e}±0.059	1.471 ^{bcd} ± 0.274	0.674 ^{ab} ± 0.044
5	57.568 ^{d} ± 0.443	10.267^{a}±0.231	0.790^{e}±0.024	1.390 ^{cd} ± 0.275	0.650 ^{ab} ± 0.042
6	58.485^{c}±0.196	7.867^{e}±0.462	0.828 ^{cd} ± 0.092	1.479 ^{bcd} ± 0.232	0.673 ^{ab} ± 0.036
7	59.674^{a}±0.301	9.067^{c}±0.231	0.857 ^{bc}±0.124	1.906^{a}±0.159	0.738^{a}±0.016
8	59.713^{a}±0.578	6.667 ^{h} ± 0.611	0.795^{e}±0.009	1.575 ^{h} ± 0.501	0.690 ^{ab} ± 0.072
9	53.758^{f}±0.660	7.733^{f}±0.611	0.909^{a}±0.081	1.377 ^{d} ± 0.317	0.610 ^{b} ± 0.059

Note: Different superscript letters in each of indicators mean significant differences at 0.05 level ($p < 0.05$, $n = 3$).

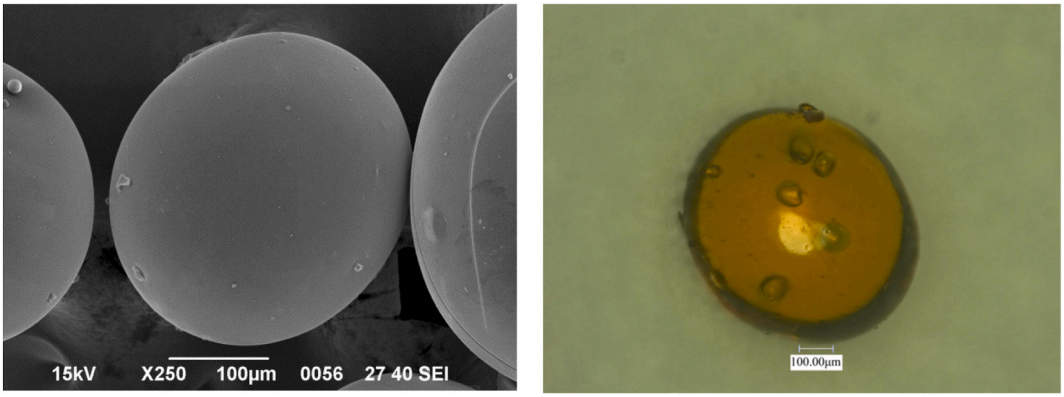

Fig. 1. SEM image (a) and three-dimensional super depth of field microscopy image (b) of CS-CCMR.

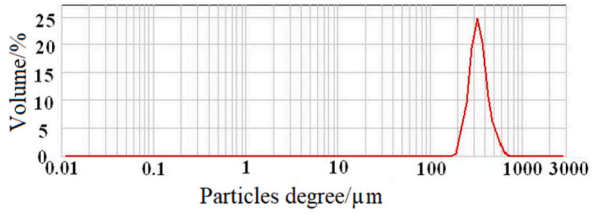

Fig. 2. CS-CCMR particle size distribution.

explored.

The physical properties of CS-CCMR and CSMR are shown in Table 8. The moisture content of CS-CCMR was slightly higher than that of CSMR. This may be because CS-CCMR has a smaller particle size, larger specific surface area, and greater bound water compared with CSMR. In addition, the Ce(IV) present in CS-CCMR, with its high charge and ion potential, can coordinate with water molecules and contribute to the moisture content. The concentration of free aldehyde groups in CS-CCMR was less than that of CSMR, which may be due to coordination between the aldehyde oxygen atom and Ce(IV) during the cross-linking process. Similarly, during cross-linking, Ce(IV) interacts with the oxygen atoms of free aldehyde groups and the amino and hydroxyl groups of chitosan, which makes the cross-linking rate of glutaraldehyde and chitosan less than that of CSMR, and the crosslinking degree of CS-CCMR is less than that of CSMR. The presence of Ce(IV) in CS-CCMR results in greater skeleton density and pore degree than those of CSMR. The weak basic exchange capacity of CS-CCMR was greater than that of CSMR, since the Ce(IV) in CS-CCMR will also react with a certain amount of weak base.

The concentrations of rare earth ions in chitosan, CSMR and CS-CCMR are shown in Table 9. The cerium content of CS-CCMR was much higher than that of CSMR or chitosan, while the concentrations of other rare earth elements were similar in all three materials. This is due to the addition of ceric ammonium nitrate in the preparation of CS-CCMR, and the formation of complexes with the amino or acetylamino groups of chitosan. In general, amino groups are more nucleophilic than hydroxyl groups, so the metal complexes formed by amino-containing glycosamines are much more stable than those formed by neutral polysaccharide molecules [49]. Amino-containing polysaccharides such as chitosan, heparin and other species containing nucleophilic amino groups, can complex many metal ions, including Cu^{2+}, Fe^{3+}, Ag^{+}, and Mg^{2+} [18,50,51]. Moreover, when chitosan is modified, such as by addition of cross-linking reagents (e.g., glutaraldehyde, epichlorohydrin, ethylene glycol diglycidyl ether, iminodiacetic acid, nitrous diacetic acid, hexamethylene diisocyanate), the chitosan can be partially crosslinked and immobilized to form a sieve. Thus, the hydrophilicity

Table 8
Physical properties of CS-CCMR and CSMR.

Physical properties	CS-CCMR	CSMR
Moisture Content (%)	59.674 ± 0.301	51.982 ± 1.944
Cross-Linking Degree (%)	9.067 ± 0.231	13.581 ± 0.677
Pile-up Density (g/mL)	0.857 ± 0.124	0.862 ± 0.007
Skeleton Density (g/cm^3)	1.906 ± 0.159	1.212 ± 0.453
Pore Degree	0.738 ± 0.016	0.554 ± 0.097
Free Aldehyde Group Content (mmol/g)	0.233 ± 0.012	0.315 ± 0.009
Weak Basic Exchange Capacity (mmol/g)	1.507 ± 0.083	1.311 ± 0.084

Table 9
Rare earth concentrations in CS-CCMR and CSMR.

Rare Earth Elements	Chitosan (mg/g)	CSMR (mg/g)	CS-CCMR (mg/g)
Cerium (Ce)	0.0046	0.0017	4.5070
Dysprosium (Dy)	0.0000	0.0000	0.0023
Erbium (Er)	0.0060	0.0000	0.0000
Europium (Eu)	0.0000	0.0000	0.0000
Gadolinium (Gd)	0.0014	0.0014	0.0011
Holmium (Ho)	0.0000	0.0000	0.0000
Lanthanum (La)	0.0006	0.0001	0.0002
Lutetium (Lu)	0.0000	0.0000	0.0001
Neodymium (Nd)	0.0004	0.0000	0.0000
Praseodymium (Pr)	0.0000	0.0000	0.0000
Scandium (Sc)	0.0005	0.0003	0.0037
Samarium (Sm)	0.0013	0.0009	0.0094
Terbium (Tb)	0.0000	0.0000	0.0011
Thulium (Tm)	0.0000	0.0001	0.0000
Yttrium (Y)	0.0001	0.0001	0.0000
Ytterbium (Yb)	0.0000	0.0000	0.0001

and pore degree of the chitosan molecule are changed, and the metal bonding capacity of the cross-linked molecule is greatly enhanced [52,53]. Consequently, CS-CCMR contains a higher concentration of Ce(IV).

3.3.2. Fluorescence spectra

The study of lanthanide chelators has attracted much attention mainly because of their potential applications, such as NMR transfer reagents, laser materials and fluorescent markers for fluorescence immunoassays [54,55]. Emission spectra were obtained by scanning samples excited at a wavelength of 250 nm (Fig. 3.). Five CS-CCMR samples were prepared using different amounts of ceric ammonium nitrate (samples 2–6 in Fig. 3.). The spectrum of ceric ammonium nitrate contained the largest absorption peak at 350 nm. The same absorption peak at 350 nm was present in the spectra of the CS-CCMR samples, but the peak intensities decreased as the Ce(IV) content decreased. The fluorescence emission signal of cerium(IV) at 350 nm was also confirmed by Wang et al. [56]. The fluorescence spectra of CSMR and chitosan did not contain an absorption peak at 350 nm. The fluorescence emission spectra confirmed the presence of Ce (IV) in CS-CCMR, and that the concentration of Ce(IV) in CS-CCMR increased as the amount of added ceric ammonium nitrate was increased.

3.3.3. XRD analysis

The XRD patterns of chitosan, CSMR and CS-CCMR are shown in Fig. 4. Chitosan is a biopolymer formed by deacetylation of chitin. It contains active hydroxyl and free amino groups, so it can form intrachain hydrogen bonds in the same way that chitin does [57]. The

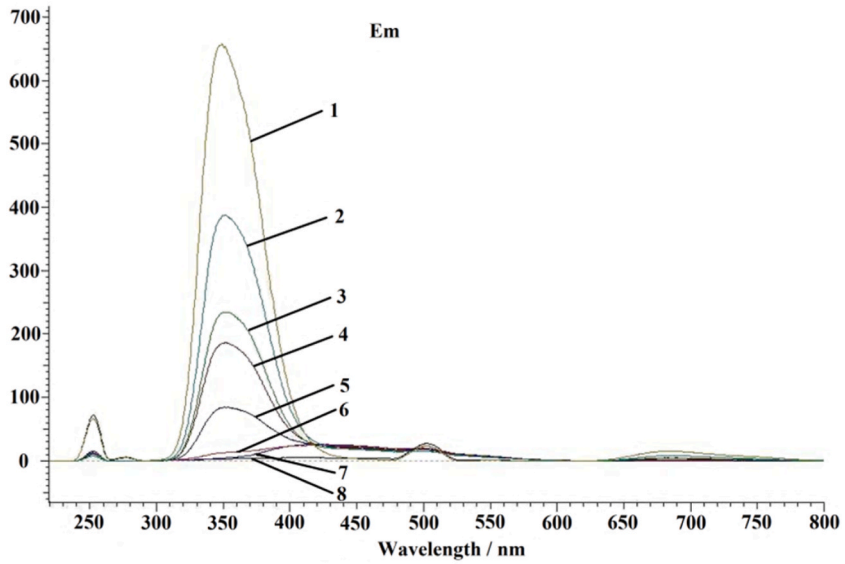

Fig. 3. Fluorescence spectra of ceric ammonium nitrate (1), CS-CCMR (2) (2.0 %, *w/v*), CS-CCMR (3) (1.5 %, *w/v*), CS-CCMR (4) (1.0 %, *w/v*), CS-CCMR (5) (0.5 %, *w/v*), CS-CCMR (6) (0.1 %, *w/v*), CSMR (7), chitosan (8). (The percentage content in the CS-CCMR sample is the amount of ceric ammonium nitrate added during its preparation).

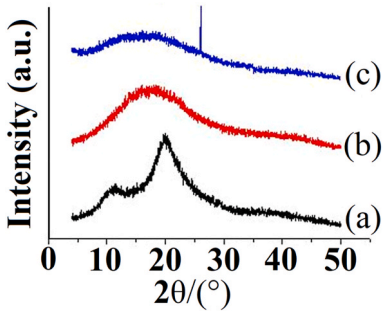

Fig. 4. X-ray diffraction patterns of chitosan (a), CSMR (b) and CS-CCMR (c).

two hydrogen bonds in the chitin chain are between the C_3 hydroxyl group and C_5 oxygen atom, and between the C_6 hydroxyl group and the carbonyl group. The two hydrogen bonds in the chitosan chain are between the C_3 hydroxyl and C_5 oxygen atom, and between the C_6 hydroxyl and amino nitrogen atom, so chitosan has greater crystallinity. The XRD pattern of chitosan indicated the presence of two different monoclinic crystal forms, namely Form I (2θ at about 10°) and Form II (2θ at about 20°) [58]. A 2θ value of 10°–20° is in the amorphous region, suggesting a small package of hydrophilic, water-rich, nitrogen-binding sites and C_6 alcohol hydroxyl groups of the polysaccharide ring [59]. During the preparation of CSMR, chitosan undergoes acetic acid dissolution and cross-linking, which will break the strong hydrogen bonding between chitosan molecules and destroy the regularity of the molecular chain. At the same time, cross-linking will restrict the mobility of the polymer molecules, resulting in reduced crystallinity. The diffraction peak at 10° in the XRD pattern of chitosan, disappeared completely in the XRD pattern of CSMR, the relative intensity of the diffraction peak at 20° was clearly decreased, and the amorphous area increased. The results indicated reduced crystallinity of CSMR, and that the amino group of chitosan was converted into a Schiff base to form the cross-linked product. In the XRD pattern of CS-CCMR the diffraction peak of 10° disappeared completely, and the relative intensity of the diffraction peak of 20° decreased further compared with that in the XRD pattern of CSMR. However, there was a new diffraction peak at $2\theta = 26.060°$. The crystal plane spacing of this diffraction peak was $d = 3.4165$, which corresponds to the diffraction peak at 25.940° ($d = 3.4320$) in the XRD pattern of ceric ammonium nitrate. The XRD patterns of cerium-modified chitosan nanoparticles prepared by Zhang et al. contained a diffraction peak due to CeO_2 at $2\theta = 28.5°$ [60]. These are characteristic diffraction peaks of cerium, demonstrating the presence of cerium in CS-CCMR. In addition, the crystallinity of CS-CCMR was further decreased due to the coordination of cerium ions with chitosan in the hydrophilic amorphous region, which was further increased in the XRD pattern relative to that in the CSMR pattern.

3.3.4. Fourier transform infrared (FTIR) analysis

In the FTIR spectra of chitosan, CSMR and CS-CCMR (Fig. 5.), the stretching vibration absorption peaks of ν(O–H) and ν(N–H) overlap to form broad peaks located at 3444.86, 3420.21 and 3419.36 cm^{-1}, respectively. It can be seen that the peaks gradually shifted towards shorter wave number, which may be due to the increased number of Schiff base bonds in CSMR and CS-CCMR, leading to hydrogen bonding and red shift of the hydroxyl stretching vibration peak. The strength of the ν(CH_3) stretching vibration absorption peak in chitosan, CSMR and CS-CCMR gradually increased, while the strength of the ν(CH_2) stretching vibration absorption peak gradually decreased. This may be due to the involvement of the C_6 hydroxyl group in cross-linking or increased steric hindrance of the molecular chain after formation of the chitosan spherical resin. The spectra of both CSMR and CS-CCMR contained peaks at 1716.10 cm^{-1}, indicating the presence of unreacted aldehyde groups in the two resins. The characteristic absorption peak of the amino group and the amide I peak near 1651.32 and 1600 cm^{-1}, and the amide II peak near 1540 cm^{-1} disappeared from the spectrum of CS-CCMR.

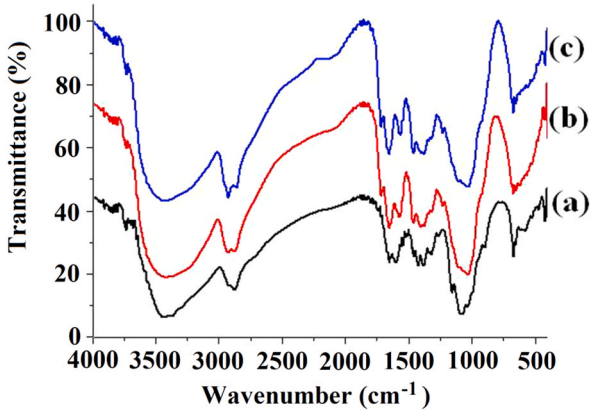

Fig. 5. FTIR spectrum of chitosan (a), CSMR (b) and CS-CCMR (c).

An absorption peak corresponding to the stretching vibration of the Schiff base ν(C═N) appeared at 1562.04 cm^{-1}. It is apparent that the amino group and part of the acetylamino group of chitosan are involved in the cross-linking reaction to form a –C═N bond. The absorption peak of the CS-CCMR Schiff base was red-shifted relative to that of the CSMR Schiff base. It is possible that an N–Ce bond is formed in CS-CCMR by coordination of Ce(IV) with the amino group, which competes with glutaraldehyde and results in the red shift of the Schiff base absorption peak. In CS-CCMR, the absorption peaks corresponding to $–CH_2$ bending and rocking vibrations, $–CH_3$ symmetric deformation vibration, and $–CH_2$ deformation vibration moved to lower frequencies 1400.09, 1378.66 and 1319.09 cm^{-1}, respectively. Compared with the spectrum of CSMR, the $–CH_2$ bending vibration and rocking vibration absorption peaks were basically unchanged, the $–CH_3$ symmetric and $–CH_2$ deformation vibration peaks were slightly blue-shifted, and the intensity of the $–CH_3$ symmetric deformation vibration peak was increased. The strength of the ν(C–O) stretching vibration of C_6–OH in CS-CCMR decreased significantly, which may be due to reaction between the aldehyde group of glutaraldehyde and the hydroxyl group of the primary alcohol. It may also be due to the change of molecular space structure of chitosan after cross-linking. The absorption peak corresponding to the ν(C–O) stretching vibration of C_3–OH blue-shifted to 1035.13 cm^{-1} relative to CSMR. The glycoside bond ν(C–O–C) peak moved to 1103.10 cm^{-1} in the spectrum of CS-CCMR. The intensity of the characteristic absorption peak of β-D-glucopyranoside decreased significantly. These changes are due to glutaraldehyde cross-linking the chitosan amino or acetylamino groups or the formation of Schiff base, such that the crystallinity of chitosan is decreased. In general, there are two models for the formation of coordination compounds between chitosan and metal ions [61]. One is the bridge model, in which the metal ion binds to several nitrogen or oxygen atoms from the same or different chains. The other is the suspension model, in which the metal ion bonds with the amino group and becomes the suspension group. Amino groups are thought to form coordination bonds with metal ions, and each glucose unit in chitosan has a unique amino coordination site. Coordination bonds are formed between the free electron pair of the ligand (amino group) and the empty orbital of the metal ion [62]. The new peak (548.55 cm^{-1}) in the infrared spectrum of CS-CCMR corresponds to the N–Ce stretching vibration peak, which indicates that coordination between Ce(IV) and chitosan has occurred, but does not reveal which coordination model it belongs to. In addition, the CS-CCMR infrared spectrum contains a peak due to ν(Ce–O) at 451.69 cm^{-1}, which is the coordination bond between C_6–OH and Ce(IV). The FTIR spectrum of hybrid chitosan cerium oxide nanoparticles prepared by Senthilkumar et al. contained cerium absorption peaks at 429.48 and 562.54 cm^{-1} [63]. The characteristic Ce absorption peak in the FTIR spectrum of CS-CCMR in this study was consistent with the above results, confirming the presence of Ce (IV) in CS-CCMR.

3.3.5. Differential scanning calorimetry (DSC) results

Fig. 6 shows DSC curves of chitosan, CSMR and CS-CCMR. The first heating stage curve for CS-CCMR showed that the endothermic peak started at 55.43 °C, ended at 112.16 °C, and the change in enthalpy, ΔH, was 95.66 J/g (Fig. 6(c)). The corresponding data for chitosan and CSMR were 57.06 °C, 82.88 °C, and 40.49 J/g (Fig. 6(a)), and 39.93 °C, 87.74 °C, and 63.41 J/g (Fig. 6(b)), respectively. The endothermic peak at this stage is mainly caused by dehydration of the chitosan macromolecule [64]. According to the experimental data, the maximum of the endothermic peak and the enthalpy for loss of water molecules increased gradually for chitosan, CSMR and CS-CCMR. This is because water molecules in chitosan mainly form hydrogen bonds with amino groups, and the energy required to break these hydrogen bonds is low. Some amino groups in CSMR have reacted with glutaraldehyde to form a Schiff base, so water molecules preferentially hydrogen bond to the hydroxyl group, which requires higher energy to break. Therefore, the enthalpy of absorption of CSMR is higher than that of chitosan. In CS-CCMR, the amino group not only reacts with glutaraldehyde to form a Schiff base, but also coordinates with Ce(IV), so water molecules can hardly bond with the amino group, but can bond with the hydroxyl group. In addition, Ce(IV) also binds to water molecules because of its high charge and ion potential. Thus, loss of water from CS-CCMR necessitates breaking the hydrogen bond between water and the hydroxyl group and the bond between Ce(IV) and water. Therefore, CS-CCMR requires more energy than chitosan or CSMR to lose water.

The second heating stage shows that the exothermic peak of CS-CCMR started at 224.68 °C, ended at 295.36 °C, and the exothermic enthalpy was 135.00 J/g (Fig. 6(c)). The corresponding experimental data for chitosan and CSMR were 288.58 °C, 326.09 °C, and 124.20 J/g (Fig. 6(b)), and 215.36 °C, 276.68 °C, and 85.63 J/g (Fig. 6(a)), respectively. The exothermic peak at this stage is related to thermal and oxidative decomposition of chitosan and the volatilization and elimination of volatile products. The thermal degradation

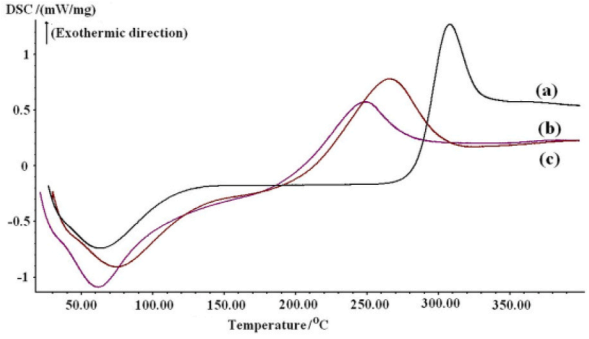

Fig. 6. DSC curves of chitosan (a), CSMR (b) and CS-CCMR (c).

temperature decreased in the order of chitosan, CS-CCMR and CSMR. There are two types of hydrogen bond in the chitosan chain, namely, the hydrogen bond between the C_3 hydroxyl and C_5 oxygen atom and the hydrogen bond between the C_6 hydroxyl and amino nitrogen atom. Therefore, chitosan has good crystallinity and thermal stability. In CSMR, the formation of a Schiff base between the amino group and glutaraldehyde breaks the hydrogen bond in the chitosan chain, which decreases the crystallinity of chitosan, thus affecting its thermal stability. In CS-CCMR, the Schiff base formed between the amino group and glutaraldehyde also breaks the hydrogen bond in the chitosan chain, resulting in decreased crystallinity of chitosan. However, Ce(IV) coordinates with the amino group, which improves thermal stability. Therefore, the thermal degradation temperature of CS-CCMR is slightly higher than that of CSMR. The glass transition temperature of chitosan was 290.05–300.60 °C, that of CS-CCMR was less than that of chitosan, at 236.88–247.37 °C, and that of CSMR was smallest, at 219.59–223.22 °C. This also demonstrates the relationship between their thermal stabilities.

3.3.6. Elemental analysis results

The necessary conditions for formation of the complex are that the general coordination body has lone electron pairs and the central ion has empty valence electron orbitals. The higher the charge of the central ion and the larger the radius are, the more ligands that can be accommodated around it. However, if the ligand is large, the formation of high coordination number will be affected by steric hindrance. In addition, the arrangement of electrons outside the core and the hybridization state of the central ion also affect the coordination number, which is closely related to the hybridization state and spatial configuration of the complex ion [65]. Ce(IV) has a radius of 0.101 nm, an outer electron layer configuration of $6s^2 4f^1 5d^1$, an open-shell free 4f electron and a non-spherical charge distribution. Therefore, Ce(IV) readily forms complexes with ligands. The CSMR, CS-CCMR and chitosan elemental analysis results are provided in Table 10. The carbon content of CSMR was higher than that of chitosan because cross-linking increases the carbon content by introduction of glutaraldehyde. For the same reason, the carbon content of CS-CCMR was also higher than that of chitosan. However, the carbon content of CS-CCMR was lower than that of CSMR because CS-CCMR contains Ce(IV). Thus, the presence of Ce (IV) in addition to glutaraldehyde in the chitosan chain makes the carbon content of CS-CCMR less than that of CSMR. The C/N ratio calculated in Table 10 illustrates the relationship between them.

3.4. Results and discussion of hydrolytic activity

3.4.1. Hydrolysis of PNPP2Na results and discussion

3.4.1.1. Hydrolysis of PNPP2Na. The molecular structure of PNPP2Na contains a phosphate ester bond, and detection of its hydrolysate, *p*-nitrophenol, is simple and rapid. *p*-Nitrophenol is light yellow with maximum absorption at 405 nm, so no color reaction is required. The hydrolysis product can be determined by reading the absorption value directly using a UV–Vis photometer. Therefore, PNPP2Na serves as a model compound for phosphate ester bond hydrolysis of CS-CCMR substrates. Fig. 7 shows the results of PNPP2Na hydrolysis. CSMR had no effect on degradation of PNPP2Na, and its absorption value was the same as that of PNPP2Na, but degradation of PNPP2Na by CS-CCMR was much greater than that of PNPP2Na alone. This result is consistent with that of the hydrolysis of the disodium salt of bis(4-nitrophenyl)phosphate BNPP by Ce-Doped carbon dots (CeCDs) [23]. They found that Ce-free CDs had no hydrolysis activity on BNPP, while Ce played an important role in the hydrolysis of BNPP. Therefore, CS-CCMR can be regarded as a phosphatase mimetic for hydrolysis of PNPP2Na.

3.4.1.2. Exploration of the mechanism of PNPP2Na hydrolysis. The mechanism of phosphate ester hydrolysis by acid or alkaline phosphatase in vivo is that the active group of the phosphatase interacts with the oxygen atom of the phosphate ester bond, then attacks the phosphorus atom to cleave the P–O bond under moderate conditions. The possible mechanism for cleavage of the P–O bond by CS-CCMR can be divided into two steps. The first step is charge neutralization, where Ce(IV) neutralizes the negative charge of the PNPP2Na phosphate oxygen with a positive charge and combines with the two negatively charged oxygens to weaken the P–O bond. The second step is nucleophilic substitution. Dissociated hydroxyl groups from water molecules in solution bind to Ce(IV), which then participate in nucleophilic attack of the P–O bond to break it and release the *p*-nitrophenol hydrolysate (Fig. 8). Matsumiya et al. investigated the hydrolysis of PNPP2Na by cerium(IV)-thiacalix[4]arene complexes [66]. They found that binuclear Ce(IV) complexes exhibited four times greater hydrolytic activity than mononuclear Ce(IV) complexes. In this hydrolysis reaction, cerium(IV)-thiacalix [4]arene complexes act like alkaline phosphatase. In another study, the hydrolytic activity of cerium oxide nanoparticles (CNPs) on phosphate ester bonds in phosphate representatives such as PNPP2Na, adenosine triphosphate (ATP), O-phospho-L-tyrosine, and DNA was investigated [44]. The authors used computational modeling to explore the mechanism of dephosphorylation by CNPs. Computational modeling showed that the transition state in PNPP2Na hydrolysis was very similar to the transition state of nucleophilic substitution of aliphatic carbon atoms. In other words, the hydroxyl groups on the surface of CNPs must be protonated. In this study,

Table 10
Elemental analyses of chitosan, CSMR and CS-CCMR.

	N (%)	C (%)	H (%)	C/N
Chitosan	7.792	42.160	6.950	5.411
CSMR	4.523	48.005	6.795	10.614
CS-CCMR	4.929	44.210	6.699	8.969

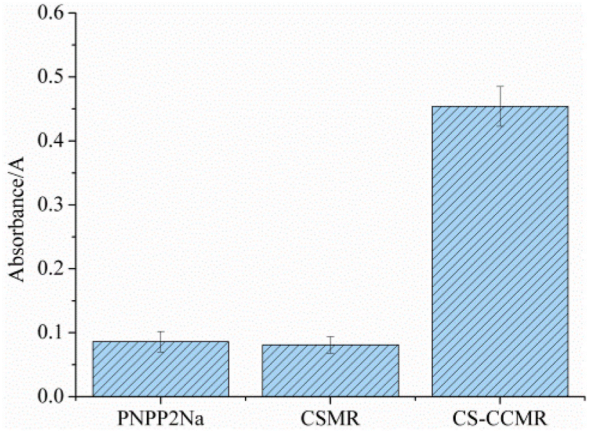

Fig. 7. PNPP2Na hydrolysis (n = 3).

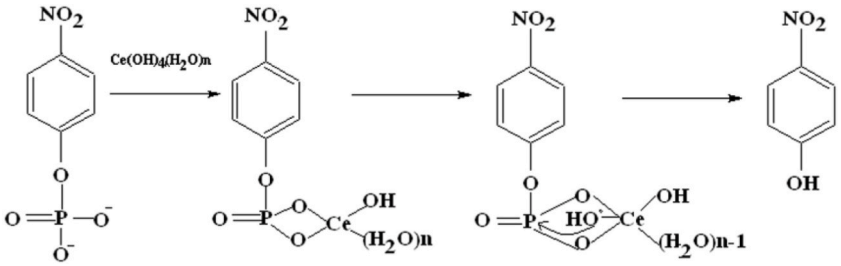

Fig. 8. Schematic mechanism of PNPP2Na phosphate bond hydrolysis by CS-CCMR.

CS-CCMR had a good hydrolytic effect on PNPP2Na, which was consistent with the results of the two studies. Furthermore, the inferred mechanism of PNPP2Na hydrolysis by CS-CCMR is similar to that of dephosphorylation simulated by computational modeling, which requires nucleophilic substitution. Based on the discovery of its phosphate ester hydrolytic properties, CS-CCMR was hypothesized to be applicable to hydrolysis of other phosphate ester-containing compounds, such as organophosphorus pesticides.

3.4.2. Results and discussion on hydrolysis of five organophosphorus pesticides

3.4.2.1. Hydrolysis of organophosphorus pesticides. Organophosphorus pesticides are a class of organophosphorus compound that contain C–P, C–O–P, C–S–P or C–N–P in their molecular structures. Due to lack of scientific knowledge, or blind overuse of organophosphorus pesticides to achieve maximum yields, organophosphorus pesticide residues in vegetables, fruits and other food products have become a key problem affecting the agricultural industry. In recent years, increasing attention has been paid to solving the issue

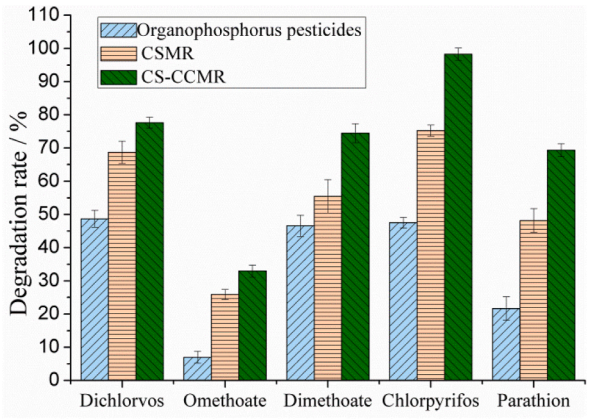

Fig. 9. Degradation of 5 organophosphorus pesticides (n = 3).

of organophosphorus pesticide residues, and many methods for their degradation, such as physical [67], chemical [68], biological [69] and polysaccharide metal complex degradation [70], have been studied. In general, degradation of organophosphorus pesticides under different environmental conditions refers to their conversion from harmful molecules to non-toxic small molecules, such as CO_2, PO_4^{3-} and H_2O. The degradation process is divided into three stages. The first stage is disappearance of the characteristic features of organophosphorus pesticides. The second stage is that the degradation products no longer pollute the environment. The final stage is the complete conversion of organophosphorus pesticides into inorganic CO_2, PO_4^{3-} and H_2O species. In this study, CSMR and CS-CCMR were used to treat organophosphorus pesticide solutions, and the results are shown in Fig. 9.

Under the experimental conditions, each of the five organophosphorus pesticides was degraded without addition of CSMR or CS-CCMR. There was more degradation when CSMR was added and CS-CCMR was better than CSMR because CS-CCMR is able to hydrolyze phosphate ester bonds. So, of all the processes, CS-CCMR gave the best results. For example, the degradation rate of chlorpyrifos by CS-CCMR was 98.31 %, which was 50.79 % higher than that by itself (47.52 %). On the other hand, the degradation rate of chlorpyrifos by CeCDs was 74.50 % [23]. This showed CS-CCMR had a good degradation effect on chlorpyrifos.

3.4.2.2. Mechanism of organophosphorus pesticide degradation. The hydrolytic activity of lanthanide coordination compounds, especially Ce(IV), is much higher than that of other metal ions. For example, some sugars and their derivatives, such as mannitol, isomaltose, dextran, and fucoidan, form water-soluble complexes with Ce(IV) that can hydrolyze phosphate bonds of plasmid DNA [71]. In recent years, some polysaccharide-Ce(IV) complexes, such as seaweed polysaccharide-Ce(IV) complex [72], agarose-Ce(IV) complex resin microspheres [73], chitosan-Ce(IV) complex resin microspheres [39] and chitosan-Ce(IV) complex film-forming materials [70], have been synthesized and used to degrade organophosphorus pesticides. In this study, the advantage of CS-CCMR is that it is stable, insoluble in solution and can't swell too much. Most importantly, Ce(IV)s are bound to chitosan by coordination bonds and are very stable in solution, so Ce(IV)s do not dissociate into the solution. This is the main difference and advantage compared to existing polysaccharide-Ce(IV) complexes or sugar-Ce(IV) complexes solution. CS-CCMR is more suitable for degradation of organophosphorus pesticides in solution, and is easily separated from solution without damaging the properties of the solution itself. In general, parathion is used as an example to deduce the possible degradation mechanism of organophosphorus pesticides by CS-CCMR. The mass spectrum of parathion determined by gas chromatography-mass spectrometry (GC-MS) is shown in Fig. 10.

The degradation of parathion is divided into several stages. First, parathion is converted into aminoparathion (Fig. 11(a)). During this stage, the positive charge of Ce(IV) in the chitosan-Ce(IV) complex is combined with the negative charge of the two oxygen atoms of the nitro group in the parathion molecule due to the high electron absorption properties of Ce(IV). As the electron cloud around the nitro-nitrogen atom moves through the two oxygen atoms toward Ce(IV), the N═O intensity decreases and is cut off. The nitro oxygen atoms are then replaced by H^+ from the active water molecules in solution, and the nitro group is converted to an amino group. Secondly, aminoparathion is degraded to diazinphos (Fig. 11(b)). During this stage, the combination of the positive charge of Ce(IV) in CS-CCMR with the negative charge of the oxygen atom of the *p*-aminophenol group weakens the P–O bond. At the same time, the hydroxyl group of the active water molecule in solution binds to Ce(IV) and participates in nucleophilic attack of the P–O bond, causing it to break. The two diethyl thiophosphates combine to form diazinon. Finally, through a series of reactions, such as P═S bond cleavage, the final degradation products, including PO_4^{3-} and SO_4^{2-}, are generated. The inorganic phosphorus converted from parathion can be detected at 460 nm using the blue molybdate method, and SO_4^{2-} in the degradation product can be added to the parathion degradation solution to produce a white precipitate. From this mechanism, it can be inferred that CS-CCMR is suitable for the removal of organophosphorus pesticides and other substances containing phosphate ester bonds in solution. On the one hand, CS-CCMR is a kind of microsphere resin with smooth, dense and porous surface that does not dissolve and swell excessively in solution. Moreover, Ce (IV) forms a stable complex with chitosan, and it can't be dissociated from the microsphere resin when phosphate ester bonds is hydrolyzed. This suggests that CS-CCMR is stable, renewable and reusable. On the other hand, in practical application, CS-CCMR is installed in the separation column. When liquid flows through the CS-CCMR column, organophosphorus pesticides or other substances containing phosphate bonds in the liquid can be effectively degraded.

In recent years, increasing attention has been paid to the excellent activity of Ce(IV) in the hydrolysis of phosphate ester bonds. Kassai et al. compared hydrolysis of phosphatidylcholine using twelve different metal ions and found that the reactivity of Ce(IV) was remarkable [74]. Furthermore, the hydrolytic efficiency of Ce(IV) on phosphatidylcholine at 37 °C and pH4.8 was 1.8 times greater than that at pH7.2. This suggests that a complex of Ce(IV) could be used as a therapeutic drug to treat symptoms caused by phosphatidylcholine accumulation. Williams et al. further optimized the hydrolysis of phosphatidylcholine with Ce(IV) [75]. They used the chelating agent bis-tris propane (BTP) to produce a homogeneous solution of Ce(IV), which had hydrolytic efficiency 5.7 times greater at pH4.8 than at pH7.2. It can be seen that Ce(IV) complex can play a more effective role in the stable state of hydrolysis phosphate ester bonds. Organophosphorus pesticides, such as phosphatidylcholine, have phosphate ester bonds in their structures and can also be hydrolyzed by Ce(IV) complexes. Wu et al. prepared a Zn(II)–Ce(IV) chitosan complex film-forming material. The material was used for film-covered storage of Chinese jujube fruits, and its effects on organophosphorus pesticides during storage were studied [55]. The results showed that the degradation rates of chlorpyrifos and parathion were increased by 30.18 % and 17.02 %, respectively. Yu et al. tried to hydrolyze organophosphorus pesticides in aqueous solution or fruit and vegetable juice with prepared resins of complexes from agarose-Ce^{4+} (RCA-Ce) and chitosan- Ce^{4+} (RCC-Ce) [39]. In experiments using RCA-Ce, there was 32.39 %, 27.12 % and 46.62 % degradation of methamidophos, omethoate and chlorpyrifos, respectively; there was 35.45 % and 38.28 % degradation of methamidophos and chlorpyrifos, respectively, in soybean sprout juice; and there was 59.76 % degradation of chlorpyrifos in tea extract. There was 30.35 % and 52.57 % degradation of methamidophos and parathionmethyl, respectively, in apple juice when using RCC-Ce. In this study, degradation of 5 organophosphorus pesticides (dichlorvos, omethoate, dimethoate, chlorpyrifos and parathion) by

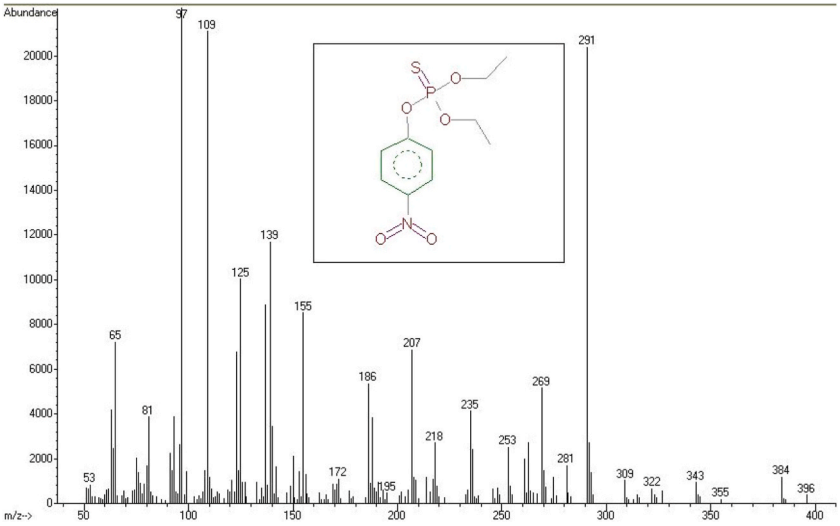

Fig. 10. Mass spectrum of parathion.

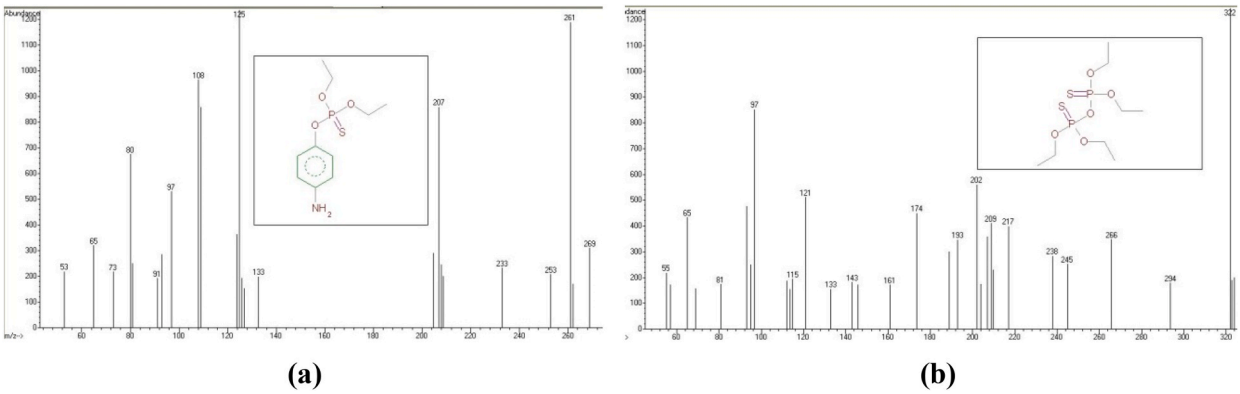

Fig. 11. Mass spectra of parathion degradation by chitosan-cerium complex.

CS-CCMR was increased, relative to the pesticides alone, to 28.96 %, 25.96 %, 27.89 %, 50.78 % and 47.71 %, respectively. This result proves that Ce(IV) has hydrolytic activity towards phosphate ester bonds, which is consistent with the above results.

In this study, the mechanism of parathion degradation was studied. The results showed that degradation of organophosphorus pesticides was similar to that of PNPP2Na, which consisted of two steps: charge neutralization and nucleophilic substitution. The ability of CS-CCMR to degrade phosphate ester bonds is attributed to the fact that Ce(IV) is a Lewis acid, and that some common electron donor atoms such as oxygen, nitrogen and sulfur can form coordination bonds with Ce(IV). The charge neutralization in the first step of the degradation pathway is then easily achieved. Desloges et al. investigated Zn^{2+}-catalyzed methanolysis of the organophosphorus pesticides paraoxon and fenitrothion [76]. The mechanism that they suggested was that the active form of the metal-ion catalyst was always a metal-hydroxyl species, which usually reacted with the substrate through a 4-coordinated transition state. The metal ions act not only as transfer coordination-OH nucleophiles, but also as Lewis acids to coordinate P–O units. Wang et al. used bisulfite-activated manganese dioxide to degrade organophosphorus pesticides and studied the transformation pathway of methyl parathion degradation [77]. First, methyl parathion is adsorbed by the activated manganese dioxide. Manganese coordinates with the sulfur atom of the P═S bond to enhance the electrophilicity of the P atom to make it more susceptible to nucleophilic attack. Next, a strong nucleophilic reagent (MnOH) on the surface of the activated manganese dioxide attacks the P atom, causing cleavage of the P–O–aryl bond and release of the main hydrolysate, *p*-nitrophenol, and O,O-dimethyl O-hydrogen phosphorothioate. The degradation pathway of organophosphorus pesticides deduced in the above two studies is consistent with the research on parathion in this study. This provides a theoretical basis for application of CS-CCMR in the degradation of substances containing phosphate ester bonds.

4. Conclusions

In this study, the preparation of CS-CCMR by reversed-phase suspension cross-linking polymerization was optimized by single

factor and orthogonal experiments, and the physicochemical properties of CS-CCMR were determined. In addition, the hydrolytic activity of CS-CCMR was also investigated. According to the physical properties, CS-CCMR is composed of dark yellow microspheres with smooth, dense and porous surfaces, and has weak basic exchange capacity. The Ce(IV) content of CS-CCMR was 4.5070 mg/g. Fluorescence spectroscopy showed that the largest absorption peak of CS-CCMR occurred at 350 nm when excited at 250 nm, which is the characteristic emission peak of Ce(IV). The XRD pattern contained a diffraction peak at $2\theta = 26.060^{\circ}$. The crystal plane spacing of this diffraction peak was $d = 3.4165$, which corresponds to the diffraction peak at 25.940° ($d = 3.4320$) in the XRD pattern of ceric ammonium nitrate. The characteristic diffraction peak demonstrates the presence of Ce(IV) in CS-CCMR. In the FTIR spectrum, a new peak (548.55 cm^{-1}) due to N–Ce stretching vibration, indicated that Ce(IV) had reacted with chitosan. In addition, a peak due to ν(Ce–O) absorption appeared at 451.69 cm^{-1}, which corresponds to the coordination bond between C_6–OH and Ce(IV). The DSC results showed that the thermal stability of CS-CCMR was improved by coordination between Ce(IV) and the amino group. The physicochemical properties and structural characterization of CS-CCMR showed that chitosan and Ce(IV) formed stable complexes, it had the characteristics of stability and renewable use of chitosan microsphere resin, as well as the advantages of hydrolysis activity of phosphate ester bonds by Ce(IV). CS-CCMR is able to hydrolyze PNPP2Na, a model compound containing a phosphate ester bond. The mechanism of hydrolysis is a combination of charge neutralization and nucleophilic substitution. The mechanism of CS-CCMR degradation of parathion is as follows: firstly, modification of the nitro group converts parathion to aminoparathion; secondly, the P–O bond of aminoparathion is cleaved to generate diazinphos; finally, degradation into PO_4^{3-}, SO_4^{2-} and other inorganic ions occurs through a series of reactions. Therefore, it can be concluded that CS-CCMR is a novel material that can remove organophosphorus pesticides from solution according to its physicochemical properties and hydrolytic activity. This will contribute to the development of a simple, effective, non-destructive process for the degradation of substances containing phosphate ester bonds. Moreover, the non-toxic, biocompatible and environmentally-friendly properties of chitosan make CS-CCMR a promising filter or clarifier for fruit and vegetable drinks, to reduce the possibility of organic phosphorus pesticide contamination. It will make a significant contribution to agricultural products and food safety. In short, this study promotes further research and application of organophosphorus pesticide pollution removal from solution. In the future, different functional groups, such as polyphenols, flavonoids and pigments, will be grafted onto CS-CCMR to develop chitosan-Ce complex microspheres with different functional activities. Then, their applications may be expanded to adsorbents for heavy metals and dyes, natural product purification carriers, sustained release agents for active substances, and other fields. The development and application of these series of CS-CCMR products are expected to play an important role in wastewater treatment, food and beverage industry, functional food raw materials production, pharmaceutical industry, chemical raw materials production and other fields. Therefore, it is very important to further explore the activity and application of CS-CCMR series functional products in the future.

Ethical statement

The study does not involve experimentation on any human or animal, nor specimens obtained from them.

Data availability

The data associated with this study is not yet deposited into a publicly available repository. Data will be made available on request.

Additional information

No additional information is available for this paper.

Funding statement

This work was supported by the Key Technology Research and Development Program of Shandong, China (Grant numbers: 2022TZXD0031 and 2023TZXD074), the Shandong Province Natural Science Foundation, China (Grant number: ZR2021MC049) and the Shandong Academy of Agricultural Sciences, China (Grant number: CXGC2023A39).

CRediT authorship contribution statement

Lina Yu: Writing – review & editing, Writing – original draft, Methodology, Formal analysis, Data curation, Conceptualization. **Yu Song:** Writing – review & editing, Supervision, Methodology, Conceptualization. **Jie Bi:** Writing – original draft, Project administration, Methodology, Data curation. **Yuan Gao:** Writing – original draft, Investigation, Data curation. **Chen Jiang:** Supervision, Investigation. **Zhen Yang:** Supervision, Funding acquisition. **Hongtao Qi:** Investigation, Conceptualization. **Honghua Yu:** Investigation, Supervision. **Weiqiang Yang:** Supervision, Resources. **Qingxuan Gong:** Supervision, Resources. **Chengren Shi:** Supervision, Project administration. **Mingqing Wang:** Writing – review & editing, Supervision, Funding acquisition, Conceptualization.

Declaration of competing interest

The authors declare that they have no known competing financial interests or personal relationships that could have appeared to influence the work reported in this paper.

References

[1] M. Pouya, T. Elham, F.S. Ying, R. Ahmad, A. Hamid, D.T. Caroline, W. Peng, L.S. Shiung, A. Mortaza, R. Hajar, T. Meisam, Comparison of shrimp waste-derived chitosan produced through conventional and microwave-assisted extraction processes: physicochemical properties and antibacterial activity assessment, Int. J. Biol. Macromol. 242 (2023) 124841, https://doi.org/10.1016/j.ijbiomac.2023.124841.

[2] Y. Liu, D. Li, M. Chen, Q. Sun, Y. Zhang, J. Zhou, T. Wang, Radical adducts formation mechanism of CH_3CO_2• and CH_3CO_3• realized decomposition of chitosan by plasma catalyzed peracetic acid, Carbohyd. Polym. 318 (2023) 121121, https://doi.org/10.1016/j.carbpol.2023.121121.

[3] M.S. Attia, M.S. Osman, A.S. Mohamed, H.A. Mahgoub, M.O. Garada, E.S. Abdelmouty, L.A.A.H. Abdel, Impact of foliar application of chitosan dissolved in different organic acids on isozymes, protein patterns and physio-biochemical characteristics of tomato grown under salinity stress, Plants 10 (2021) 388, https://doi.org/10.3390/plants10020388.

[4] X. Xing, Y. Han, H. Cheng, Biomedical applications of chitosan/silk fibroin composites: a review, Int. J. Biol. Macromol. 240 (2023) 124407, https://doi.org/10.1016/j.ijbiomac.2023.124407.

[5] R. Tao, N. Zhang, L. Zhang, T. Habumugisha, Y. Chen, Y. Lu, Y. Wang, K. Wang, Y. Wang, J. Jiang, Characterization and antivibrio activity of chitosan-citral Schiff base calcium complex for a calcium citrate sustained release antibacterial agent, Int. J. Biol. Macromol. 239 (2023) 124355, https://doi.org/10.1016/j.ijbiomac.2023.124355.

[6] M.H. Rahaman, M.A. Islam, M.M. Islam, M.A. Rahman, N.S. Alam, Biodegradable composite adsorbents of modified cellulose and chitosan to remove heavy metal ions from aqueous solution, Curr. Res. Green Sustain. Chem. 4 (2021) 100119, https://doi.org/10.1016/j.crgsc.2021.100119.

[7] R. Zhang, B. Liu, J. Ma, R. Zhu, Preparation and characterization of carboxymethyl cellulose/chitosan/alginic acid hydrogels with adjustable pore structure for adsorption of heavy metal ions, Eur. Polym. J. 179 (2022) 111577, https://doi.org/10.1016/j.eurpolymj.2022.111577.

[8] R. Shikha, L. Sohan, A. Sanjiv, J. Geetanjali, K. Sumit, Schiff base of O-carboxymethyl chitosan and its complexes with transition metal ions: syntheses, structural, antimicrobial and thermal studies, Iran. Polym. J. (Engl. Ed.) 31 (2022) 1093–1105, https://doi.org/10.1007/s13726-022-01063-7.

[9] R.N. Shinde, A.K. Pandey, R. Acharya, R. Guin, S.K. Das, N.S. Rajurkar, P.K. Pujari, Chitosan-transition metal ions complexes for selective arsenic(V) preconcentration, Water Res. 47 (2013) 3497–3506, https://doi.org/10.1016/j.watres.2013.03.059.

[10] Ł. Wujcicki, T. Mańdok, L.W. Budzińska, K. Pawlusińska, N. Szozda, G. Dudek, K. Piotrowski, R. Turczyn, M. Krzywiecki, K.A. Kazek, J. Kluczka, Cerium(IV) chitosan-based hydrogel composite for efficient adsorptive removal of phosphates (V) from aqueous solutions, Sci. Rep. 13 (2023) 13049, https://doi.org/10.1038/s41598-023-40064-1.

[11] A.A. Alshahrani, A.Q. Alorabi, M.S. Hassan, T. Amna, M. Azizi, Chitosan-functionalized hydroxyapatite-cerium oxide heterostructure: an efficient adsorbent for dyes removal and antimicrobial agent, Nanomaterials 12 (2022) 2713, https://doi.org/10.3390/nano12152713.

[12] M. Chen, M. Yu, R. Kang, H. Sun, W. Zhang, S. Wang, N. Wang, J. Wang, Removal of Pb (II) and V (V) from aqueous solution by glutaraldehyde crosslinked chitosan and nanocomposites, Chemosphere 297 (2022) 134084, https://doi.org/10.1016/j.chemosphere.2022.134084.

[13] P. Rani, R. Johar, P.S. Jassal, Adsorption of nickel (II) ions from wastewater using glutaraldehyde cross-linked magnetic chitosan beads: isotherm, kinetics and thermodynamics, Water Sci. Technol. 82 (2020) 2193–2202, https://doi.org/10.2166/wst.2020.459.

[14] A. Amjlef, S. Farsad, A. Chaoui, A. Ben Hamou, M. Ezzahery, S. Et-Taleb, N. El Alem, Effective adsorption of Orange G dye using chitosan cross-linked by glutaraldehyde and reinforced with quartz sand, Int. J. Biol. Macromol. 239 (2023) 124373, https://doi.org/10.1016/j.ijbiomac.2023.124373.

[15] Q. Liu, Y. Wang, X. Liu, S. Li, S. Ren, Z. Gao, T. Han, Z. Xu, H. Zhou, Glutaraldehyde base-cross-linked chitosan-silanol/Fe_3O_4 composite for removal of heavy metals and bacteria, Environ. Sci. Pollut. Res. 29 (2022) 69439–69449, https://doi.org/10.1007/s11356-022-20673-5.

[16] A. Webster, M.D. Halling, D.M. Grant, Metal complexation of chitosan and its glutaraldehyde cross-linked derivative, Carbohydr. Res. 342 (2007) 1189–1201, https://doi.org/10.1016/j.carres.2007.03.008.

[17] S. Rashid, C. Shen, J. Yang, J. Liu, J. Li, Preparation and properties of chitosan–metal complex: some factors influencing the adsorption capacity for dyes in aqueous solution, J. Environ. Sci. 30 (2018) 301–309, https://doi.org/10.1016/j.jes.2017.04.033.

[18] W. Liu, Y. Qin, S. Liu, R. Xing, H. Yu, X. Chen, K. Li, P. Li, C-coordinated O-carboxymethyl chitosan metal complexes: synthesis, characterization and antifungal efficacy, Int. J. Biol. Macromol. 106 (2018) 68–77, https://doi.org/10.1016/j.ijbiomac.2017.07.176.

[19] W. Liu, Y. Qin, S. Liu, R. Xing, H. Yu, X. Chen, K. Li, P. Li, Synthesis of C-coordinated O-carboxymethyl chitosan metal complexes and evaluation of their antifungal activity, Sci. Rep. 8 (2018) 4845, https://doi.org/10.1038/s41598-018-23283-9.

[20] M. Manimohan, R. Paulpandiyan, S. Pugalmani, M.A. Sithique, Biologically active Co (II), Cu (II), Zn (II) centered water soluble novel isoniazid grafted O-carboxymethyl chitosan Schiff base ligand metal complexes: synthesis, spectral characterisation and DNA nuclease activity, Int. J. Biol. Macromol. 163 (2020) 801–816, https://doi.org/10.1016/j.ijbiomac.2020.06.278.

[21] T. Vadivel, M. Dhamodaran, S. Kulathooran, S. Kavitha, K. Amirthaganesan, S. Chandrasekaran, S. Ilayaraja, S. Senguttuvan, Rhodium(III) complexes derived from complexation of metal with azomethine linkage of chitosan biopolymer Schiff base ligand: spectral, thermal, morphological and electrochemical studies, Carbohydr. Res. 487 (2020) 107878, https://doi.org/10.1016/j.carres.2019.107878.

[22] R. Antony, S. Theodore David, K. Saravanan, K. Karuppasamy, S. Balakumar, Synthesis, spectrochemical characterisation and catalytic activity of transition metal complexes derived from Schiff base modified chitosan, Spectrochim. Acta Mol. Biomol. Spectrosc. 103 (2013) 423–430, https://doi.org/10.1016/j.saa.2012.09.101.

[23] J. Du, S. Qi, J. Chen, Y. Yang, T. Fan, P. Zhang, S. Zhuo, C. Zhu, Fabrication of highly active phosphatase-like fluorescent cerium-doped carbon dots for monitoring the hydrolysis of phosphate diesters, RSC Adv. 10 (2020) 41551–41559, https://doi.org/10.1039/d0ra07429b.

[24] T. Takarada, M. Yashiro, M. Komiyama, Catalytic hydrolysis of peptides by cerium (IV), Chemistry. 6 (2000) 3906–3913, https://doi.org/10.1002/1521-3765(20001103)6:21<3906::aid-chem3906>3.3.co;2-a.

[25] M. Appu, H. Wu, H. Chen, J. Huang, Tea polyphenols mediated biogenic synthesis of chitosan-coated cerium oxide (CS/CeO) nanocomposites and their potent antimicrobial capabilities, Environ. Sci. Pollut. Res. Int. 30 (2023) 42575–42586, https://doi.org/10.1007/s11356-022-19349-x.

[26] E. Kızılkonca, E. Torlak, F.B. Erim, Preparation and characterization of antibacterial nano cerium oxide/chitosan/hydroxyethylcellulose/polyethylene glycol composite films, Int. J. Biol. Macromol. 177 (2021) 351–359, https://doi.org/10.1016/j.ijbiomac.2021.02.139.

[27] A. Sanmugam, L.K. Sellappan, S. Manoharan, A. Rameshkumar, R.S. Kumar, A.I. Almansour, N. Arumugam, H.S. Kim, D. Vikraman, Development of chitosan-based cerium and titanium oxide loaded polycaprolactone for cutaneous wound healing and antibacterial applications, Int. J. Biol. Macromol. 256 (2024) 128458, https://doi.org/10.1016/j.ijbiomac.2023.128458.

[28] L. Yildizbakan, N. Iqbal, P. Ganguly, E. Kumi-Barimah, T. Do, E. Jones, P.V. Giannoudis, A. Jha, Fabrication and characterisation of the cytotoxic and antibacterial properties of chitosan-cerium oxide porous scaffolds, Antibiotics (Basel) 12 (2023) 1004, https://doi.org/10.3390/antibiotics12061004.

[29] H. Fu, P. Tan, R. Wang, S. Li, H. Liu, Y. Yang, Z. Wu, Advances in organophosphorus pesticides pollution: current status and challenges in ecotoxicological, sustainable agriculture, and degradation strategies, J. Hazard Mater. 15 (2022) 424, https://doi.org/10.1016/j.jhazmat.2021.127494.

[30] K. Seebunrueng, S. Tamuang, P. Jarujamrus, S. Saengsuwan, N. Patdhanagul, Y. Areerob, S. Sansuk, S. Srijaranai, Eco-friendly thermosensitive magnetic-molecularly-imprinted polymer adsorbent in dispersive solid-phase microextraction for gas chromatographic determination of organophosphorus pesticides in fruit samples, Food Chem. 430 (2024) 137069, https://doi.org/10.1016/j.foodchem.2023.137069.

[31] V. Elencovan, N. Yahaya, M. Raoov, N.N.M. Zain, Exploring a novel silicone surfactant-based deep eutectic solvent functionalized magnetic iron particles for the extraction of organophosphorus pesticides in vegetable samples, Food Chem. 396 (2022) 133670, https://doi.org/10.1016/j.foodchem.2022.133670.

[32] J. Zhu, J. Yu, B. Zhang, C. Li, J. Wang, J. Ji, D. Liu, R. Gao, J. Li, Y. Ma, Hydrophobic-action-driven removal of six organophosphorus pesticides from tea infusion by modified carbonized bacterial cellulose, Food Chem. 412 (2023) 135546, https://doi.org/10.1016/j.foodchem.2023.135546.

[33] T. Boontongto, Y. Santaladchaiyakit, R. Burakham, Molecularly imprinted polymer-coated paper for the selective extraction of organophosphorus pesticides from fruits, vegetables, and cereal grains, Talanta 270 (2024) 125536, https://doi.org/10.1016/j.talanta.2023.125536.

[34] S. Manafi Khoshmanesh, H. Hamishehkar, H. Razmi, Trace analysis of organophosphorus pesticide residues in fruit juices and vegetables by an electrochemically fabricated solid-phase microextraction fiber coated with a layer-by-layer graphenized graphite/graphene oxide/polyaniline nanocomposite, Anal. Methods 12 (2020) 3268–3276, https://doi.org/10.1039/d0ay00626b.
[35] X. Mu, Y. Wang, B. Qian, G. Liu, J. Xu, F. Zeng, Monitoring of organophosphorus pesticide residues in plant and vegetable tissues by a novel silver nanocluster probe, Anal. Methods 15 (2023) 762–770, https://doi.org/10.1039/d2ay01903e.
[36] M. Ghorbani, P. Mohammadi, M. Keshavarzi, M.H. Saghi, M. Mohammadi, A. Shams, M. Aghamohammadhasan, Simultaneous determination of organophosphorus pesticides residues in vegetable, fruit juice, and milk samples with magnetic dispersive micro solid-phase extraction and chromatographic method; recruitment of simplex lattice mixture design for optimization of novel sorbent composites, Anal. Chim. Acta 1178 (2021) 338802, https://doi.org/10.1016/j.aca.2021.338802.
[37] P. Sathish Kumar, B. Shobana, P. Prakash, Light harvesting enhancement through band structure engineering in graphite carbon nitride/polydopamine nanocomposite photocatalyst: addressing persistent organophosphorus pesticide pollution in water systems, Chemosphere 354 (2024) 141708, https://doi.org/10.1016/j.chemosphere.2024.141708.
[38] P. Wang, M. Luo, D. Liu, J. Zhan, X. Liu, F. Wang, Z. Zhou, P. Wang, Application of a magnetic graphene nanocomposite for organophosphorus pesticide extraction in environmental water samples, J. Chromatogr. A 1535 (2018) 9–16, https://doi.org/10.1016/j.chroma.2018.01.003.
[39] L. Yu, D. Wang, H. Li, L. Su, J. Wang, Hydrolysis activities of resins of complexes made from polysaccharides and Ce^{4+}, J. Rare Earth. 24 (spec.) (2006) 125–129.
[40] L. Yu, D. Wang, W. Hu, H. Li, M. Tang, Study on the preparation and adsorption thermodynamics of chitosan microsphere resins, Front. Chem. China 4 (2009) 160–167, https://doi.org/10.1007/s11458-009-0029-4.
[41] L. Yu, J. Bi, Y. Song, M. Wang, Isotherm, thermodynamics, and kinetics of methyl orange adsorption onto magnetic resin of chitosan microspheres, Int. J. Mol. Sci. 23 (2022) 13839, https://doi.org/10.3390/ijms232213839.
[42] H. Wang, M. Roman, Effects of chitosan molecular weight and degree of deacetylation on chitosan-cellulose nanocrystal complexes and their formation, Molecules 28 (2023) 1361, https://doi.org/10.3390/molecules28031361.
[43] H. Yu, M.H. Nguyen, K. Hadinoto, Effects of chitosan molecular weight on the physical and dissolution characteristics of amorphous curcumin-chitosan nanoparticle complex, Drug Dev. Ind. Pharm. 44 (2018) 82–88, https://doi.org/10.1080/03639045.2017.1373802.
[44] M.H. Kuchma, C.B. Komanski, J. Colon, A. Teblum, A.E. Masunov, B. Alvarado, S. Babu, S. Seal, J. Summy, C.H. Baker, Phosphate ester hydrolysis of biologically relevant molecules by cerium oxide nanoparticles, Nanomedicine 6 (2010) 738–744, https://doi.org/10.1016/j.nano.2010.05.004.
[45] S.C. Hsu, S.H. Hsu, S.W. Chang, Effect of pH on molecular structures and network of glycol chitosan, ACS Biomater. Sci. Eng. 6 (2020) 298–307, https://doi.org/10.1021/acsbiomaterials.9b01101.
[46] B. Farasati Far, M.R. Naimi-Jamal, M. Jahanbakhshi, A. Hadizadeh, S. Dehghan, S. Hadizadeh, Enhanced antibacterial activity of porous chitosan-based hydrogels crosslinked with gelatin and metal ions, Sci. Rep. 14 (2024) 7505, https://doi.org/10.1038/s41598-024-58174-9.
[47] K. Luo, Y. Gao, Y. Zhang, W. Chen, S. Tang, Chitosan/polyacrylic acid/octadecene double-crosslinked network hydrogel functionalized porous silica microspheres for multimode liquid chromatographic separation, J. Chromatogr. A 1709 (2023) 464390, https://doi.org/10.1016/j.chroma.2023.464390.
[48] J. Liang, J. Wang, S. Li, L. Xu, R. Wang, R. Chen, Y. Sun, The size-controllable preparation of chitosan/silver nanoparticle composite microsphere and its antimicrobial performance, Carbohydr. Polym. 220 (2019) 22–29, https://doi.org/10.1016/j.carbpol.2019.05.048.
[49] C. Liu, X. Wang, Z. Kong, L. Zhang, Z. Xin, X. She, J. Sun, D. Yang, D. Li, Electrostatic interaction in amino protonated chitosan-metal complex anion hydrogels: a simple approach to porous metal carbides/N-doped carbon aerogels for energy conversion, ACS Appl. Mater. Interfaces 14 (2022) 22151–22160, https://doi.org/10.1021/acsami.2c03443.
[50] H.E. Ghonam, M.A. Abu Yousef, Y.M. Gohar, R. Almeer, K.M. Barakat, A new antidiabetic foot bacteria formula from marine chitosan nanosilver-metal complex, Environ. Sci. Pollut. Res. Int. 28 (2021) 60833–60841, https://doi.org/10.1007/s11356-021-14958-4.
[51] S.B. Aziz, E.M.A. Dannoun, M.H. Hamsan, R.T. Abdulwahid, K. Mishra, M.M. Nofal, M.F.Z. Kadir, Improving EDLC device performance constructed from plasticized magnesium ion conducting chitosan based polymer electrolytes via metal complex dispersion, Membranes 11 (2021) 289, https://doi.org/10.3390/membranes11040289.
[52] L.F. Zhang, T.Y. Zhu, X. Liu, W.Q. Zhang, Simultaneous oxidation and adsorption of As(III) from water by cerium modified chitosan ultrafine nanobiosorbent, J. Hazard Mater. 308 (2016) 1–10, https://doi.org/10.1016/j.jhazmat.2016.01.015.
[53] H. Kaygusuz, E. Torlak, G. Akın-Evingür, İ. Özen, R. von Klitzing, F.B. Erim, Antimicrobial cerium ion-chitosan crosslinked alginate biopolymer films: a novel and potential wound dressing, Int. J. Biol. Macromol. 105 (2017) 1161–1165, https://doi.org/10.1016/j.ijbiomac.2017.07.144.
[54] S. Bunda, N. Lihi, Z. Szaniszló, D. Esteban-Gómez, C. Platas-Iglesias, M. Kéri, G. Papp, F.K. Kálmán, Bipyridil-based chelators for Gd(III) complexation: kinetic, structural and relaxation properties, Dalton Trans. 52 (2023) 17030–17040, https://doi.org/10.1039/d3dt02806b.
[55] R.M. Pallares, K.P. Carter, S.E. Zeltmann, T. Tratnjek, A.M. Minor, R.J. Abergel, Selective lanthanide sensing with gold nanoparticles and hydroxypyridinone chelators, Inorg. Chem. 59 (2020) 2030–2036, https://doi.org/10.1021/acs.inorgchem.9b03393.
[56] L. Wang, S. Zheng, Y. Chen, C. Li, F. Wang, Construction of Fluorescence and Colorimetric Tandem Dual-Mode Sensor by Modulating Fluorescence and Oxidase-like Activity via Valence Switching of Cerium-Based Coordination Polymer Nanoparticles for Sarcosine Detection, vol. 190, 2023, p. 157, https://doi.org/10.1007/s00604-023-05750-x.
[57] Z. Mei, P. Kuzhir, G. Godeau, Update on chitin and chitosan from insects: sources, production, characterization, and biomedical applications, Biomimetics 9 (2024) 195, https://doi.org/10.3390/biomimetics9050297.
[58] C. Xu, S. Guan, B. Wang, S. Wang, Y. Wang, C. Sun, X. Ma, T. Liu, Synthesis of protocatechuic acid grafted chitosan copolymer: structure characterization and in vitro neuroprotective potential, Int. J. Biol. Macromol. 109 (2018) 1–11, https://doi.org/10.1016/j.ijbiomac.2017.12.019.
[59] A.G. Ibrahim, A.G. Hamodin, A. Fouda, A.M. Eid, W.E. Elgammal, Fabrication and characterization of a new eco-friendly sulfonamide-chitosan derivative with enhanced antimicrobial and selective cytotoxicity properties, Sci. Rep. 14 (2024) 10228, https://doi.org/10.1038/s41598-024-60456-1.
[60] L. Zhang, T. Zhu, X. Liu, W. Zhang, Simultaneous oxidation and adsorption of As(III) from water by cerium modified chitosan ultrafine nanobiosorbent, J. Hazard Mater. 308 (2016) 1–10, https://doi.org/10.1016/j.jhazmat.2016.01.015.
[61] G. Priyadarshi, N.P. Raval, M.H. Trivedi, Microwave-assisted synthesis of cross-linked chitosan-metal oxide nanocomposite for methyl orange dye removal from unary and complex effluent matrices, Int. J. Biol. Macromol. 219 (2022) 53–67, https://doi.org/10.1016/j.ijbiomac.2022.07.239.
[62] F. Wahid, H.S. Wang, C. Zhong, L.Q. Chu, Facile fabrication of moldable antibacterial carboxymethyl chitosan supramolecular hydrogels cross-linked by metal ions complexation, Carbohydr. Polym. 165 (2017) 455–461, https://doi.org/10.1016/j.carbpol.2017.02.085.
[63] R.P. Senthilkumar, V. Bhuvaneshwari, R. Ranjithkumar, S. Sathiyavimal, V. Malayaman, B. Chandarshekar, Synthesis, characterization and antibacterial activity of hybrid chitosan-cerium oxide nanoparticles: as a bionanomaterials, Int. J. Biol. Macromol. 104 (2017) 1746–1752, https://doi.org/10.1016/j.ijbiomac.2017.03.139.
[64] M.F. Guimarães, L. Pighinelli, R.L. Paz, M. Kmiec, G. Zehetmeyer, C.M. Becker, C.F. Escobar, L.A. Dos Santos, Chemical and physical properties of nanocrystalline chitosan by the method: modified nanochitosan complex and process of obtaining modified nanochitosan, Carbohydr. Res. 493 (2020) 108035, https://doi.org/10.1016/j.carres.2020.108035.
[65] M. Gregson, E. Lu, J. McMaster, W. Lewis, A.J. Blake, S.T. Liddle, A cerium(IV)-carbon multiple bond, Angew. Chem. Int. Ed. Engl. B 52 (2013) 13016–13019, https://doi.org/10.1002/anie.201306984.
[66] H. Matsumiya, H. Nakamura, M. Hiraide, Phosphoester hydrolysis by cerium(IV)-thiacalix[4]arene complexes and its application to immunoassay, Anal. Bioanal. Chem. 394 (2009) 1471–1476, https://doi.org/10.1007/s00216-009-2798-5.
[67] T. Khedr, A.A. Hammad, A.M. Elmarsafy, E. Halawa, M. Soliman, Degradation of some organophosphorus pesticides in aqueous solution by gamma irradiation, J. Hazard Mater. 373 (2019) 23–28, https://doi.org/10.1016/j.jhazmat.2019.03.011.
[68] M. Fan, P. Zhang, C. Wang, J. Tang, H. Sun, Tailored design of three-dimensional rGOA-nZVI catalyst as an activator of persulfate for degradation of organophosphorus pesticides, J. Hazard Mater. 428 (2022) 128254, https://doi.org/10.1016/j.jhazmat.2022.128254.

[69] X. Zheng, L. Wang, L. Qi, Z. Dong, A novel organophosphorus acid anhydrolase from deep sea sediment with high degradation efficiency for organophosphorus pesticides and nerve agent, Microorganisms 10 (2022) 1112, https://doi.org/10.3390/microorganisms10061112.
[70] H. Wu, D. Wang, J. Shi, S. Xue, M. Gao, Effect of the complex of zinc(II) and cerium(IV) with chitosan on the preservation quality and degradation of organophosphorus pesticides in Chinese jujube (zizyphus jujuba mill. Cv. Dongzao), J. Agric. Food Chem. 58 (2010) 5757–5762, https://doi.org/10.1021/jf100537k.
[71] D. Wang, J. Sumaoka, C. Wang, X. Liang, M. Komiyama, Effect of complexes coordinating alginic polysaccharides with cerium on cleavage of plasmid DNA and bovine serum albumin, Journal of the Chinese Rare Earth Society (in China) 20 (2002) 283–285, https://doi.org/10.1038/sj.cr.7290132.
[72] D. Wang, J. Sun, D. Du, L. Sun, Z. Chen, C. Xue, Degradation of extraction from seaweed and its complex with rare earths for organophosphorous pesticides, J. Rare Earth. 25 (2007) 93–99.
[73] L. Yu, D. Wang, L. Su, Y. Luo, L. Sun, C. Xue, Hydrolysis activities of the particle of agarose-Ce^{4+} complex for compounds containing phosphodiester or peptide bonds, J. Ocean U. Chinese 4 (2005) 272–275, https://doi.org/10.1007/s11802-005-0047-x.
[74] M. Kassai, R. Teopipithaporn, K.B. Grant, Hydrolysis of phosphatidylcholine by cerium(IV) releases significant amounts of choline and inorganic phosphate at lysosomal pH, J. Inorg. Biochem. 105 (2011) 215–223, https://doi.org/10.1016/j.jinorgbio.2010.11.007.
[75] D.E. Williams, K. Basnet, K.B. Grant, Tuning cerium(IV)-assisted hydrolysis of phosphatidylcholine liposomes under mildly acidic and nutral conditions, Chembiochem 16 (2015) 1474–1482, https://doi.org/10.1002/cbic.201500041.
[76] W. Desloges, A.A. Neverov, R.S. Brown, Zn^{2+}-catalyzed methanolysis of phosphate triesters: a process for catalytic degradation of the organophosphorus pesticides paraoxon and fenitrothion, Inorg. Chem. 43 (2004) 6752–6761, https://doi.org/10.1021/ic030325r.
[77] J. Wang, Y. Teng, C. Zhang, X. Liao, Y. Zhai, R. Zuo, Activation of manganese dioxide with bisulfite for enhanced abiotic degradation of typical organophosphorus pesticides: kinetics and transformation pathway, Chemosphere 226 (2019) 858–864, https://doi.org/10.1016/j.chemosphere.2019.03.120.